ATP content, and results in muscle atrophy. However, this hypothesis has not been verified. In the present study, we examined mitochondrial respiratory function and morphological changes in the skeletal muscles of mice overexpressing PGC-1α and found that PGC-1α transgenic mice had markedly decreased ATP content in skeletal muscles and developed myopathy at 25 weeks of age, which recapitulates the phenotype of Luft's disease.[8–10]

Materials and Methods

Animals and Treatments

D-line mice expressed 10-fold higher PGC-1α mRNA and E-line mice expressed 13-fold higher PGC-1α mRNA in skeletal muscle compared to wild-type mice, as described in our previous study.[6] Male chimeras harboring the PGC-1 transgene were mated with pure C57BL/6J females (Tokyo Laboratory Animals Science, Tokyo, Japan) to obtain F_1 offspring. The heterozygous F_1 male offspring from this breeding were then backcrossed with purebred C57BL/6J females to obtain F_2 offspring, and this process was continued until the F_3 generation of mice was obtained. Heterozygous transgenic mice were used for the following studies.

Mice were fed a standard laboratory chow diet (CE2; Clea, Tokyo, Japan). Mice were exposed to a 12-hour light/dark cycle and maintained at a constant temperature of 22°C. The mice were cared for in accordance with "Principles of Laboratory Animal Care" (National Institutes of Health publication no. 85-23, revised 1985: *http://grants1.nih.gov/grants/olaw/references/phspol.htm*) and our institutional guidelines.

Oxygen consumption was measured with a metabolic chamber as described previously.[11] For estimation of running wheel activity, mice were housed individually in cages (9 × 22 × 9 cm) equipped with a running wheel (20-cm diameter; Shinano Co., Tokyo, Japan). Each wheel revolution was registered by a magnetic switch connected to a counter. The number of revolutions was recorded daily for 10 days.

Histological Analyses

Samples of the tibialis anterior muscle at 16 weeks of age and hindlimb at 25 weeks of age were frozen in liquid nitrogen-cooled isopentane, and transverse serial sections were stained with hematoxylin and eosin (H&E), modified Gomori trichrome, and Oil red O.[12] These sections were also analyzed by enzyme histochemistry to evaluate cytochrome *c* oxidase (COX)[13] and succinate dehydrogenase (SDH) activities.[14] For electron microscopy, extensor digitorum longus muscles from 16-week-old mice were fixed in buffered 2% isotonic glutaraldehyde (pH 7.4), postfixed in osmium tetroxide, and embedded in epoxy resin. Ultrathin sections were stained with uranyl acetate and lead nitrate and examined with an H-7000 electron microscope (Hitachi, Tokyo, Japan).

Preparation of the Mitochondrial Fraction from Skeletal Muscle

Skeletal muscles (gastrocnemius and quadriceps) from both 14-week-old wild-type and PGC-1α transgenic male mice were pooled from three mice in each group. Tissues were cut with scalpels and treated with 1 ml of protease buffer containing 0.1 mol/L KCl, 50 mmol/L Tris-HCl (pH 7.5), 5 mmol/L $MgSO_4$, 1 mmol/L ethylenediaminetetraacetic acid (EDTA), 5 mg/ml bovine serum albumin, 1 mmol/L ATP, and 2 mg/ml proteinase K for 2 minutes on ice. Tissues were then washed with ATP buffer containing 0.1 mol/L KCl, 50 mmol/L Tris-HCl (pH 7.5), 5 mmol/L $MgSO_4$, 1 mmol/L EDTA, 5 mg/ml bovine serum albumin, and 1 mmol/L ATP. The washed tissues were homogenized in 10 ml of ATP buffer with a glass/Teflon homogenizer in a power-driven Potter-Elvehjem homogenizer (Kadoguchi-Keiki, Tokyo, Japan). The homogenate was brought to 15 ml and centrifuged at 600 × *g* for 10 minutes to remove cell debris and nuclei. The supernatant was then centrifuged at 4500 × *g* for 15 minutes. The pellet was washed with KCl buffer containing 0.1 mol/L KCl, 50 mmol/L Tris-HCl (pH 7.5), 5 mmol/L $MgSO_4$, 1 mmol/L EDTA, and 5 mg/ml bovine serum albumin and centrifuged at 7000 × *g* for 15 minutes. The mitochondrial pellet was resuspended in mitochondrial buffer containing 225 mmol/L mannitol and 75 mmol/L sucrose.[15] Protein concentrations were estimated by Lowry method.[16]

Measurement of Mitochondrial Respiration

Mitochondrial respiration was measured with Biological Oxygen Monitor 5300 (Yellow Springs Instrument, Yellow Springs, OH) was performed using Clark-type oxygen electrodes.[17] Respiration buffer containing 225 mmol/L mannitol, 75 mmol/L sucrose, 10 mmol/L Tris-HCl (pH 7.2), 5 mmol/L potassium phosphate (pH 7.2), and 10 mmol/L KCl was used. Five mmol/L succinate as substrate and 100 μg of mitochondria and 5 μg/ml rotenone were added, and respiration was started by the addition of 5 mmol/L potassium succinate. State 3 respiration was started by the addition of 200 μmol/L ADP (Sigma, St. Louis, MO). Finally, 2.5 μg/ml oligomycin (Sigma) was added as an inhibitor of ATP synthetase to block all phosphorylation-related respiration.[2]

Enzymatic Activity of the Respiratory Complex

SDH activity was measured by monitoring the change in absorbance 3-(4,5-dimethylthiazol-2-yl)-2,5-diphenyl-2,4-tetrazolium bromide (MTT) at 570 nm in the presence of phenazine methosulfate with the 17 $mmol/L^{-1}cm^{-1}$ extinction coefficient for MTT.[18] Succinate-ubiquinone oxidoreductase activity was measured in the presence of 2,3–2,6-dichlorophenolindophenol (DCIP) with the 21 $mmol/L^{-1}cm^{-1}$ extinction coefficient for DCIP.[18] NADH-ubiquinone reductase activity was assayed in 50 mmol/L potassium phosphate buffer (pH 7.7), 200 μmol/L NADH, 2 mmol/L KCN, and 90 μmol/L ubiquinone-1. Oxidation of NADH was monitored at 340 nm with a $mmol/L^{-1}$ extinc-

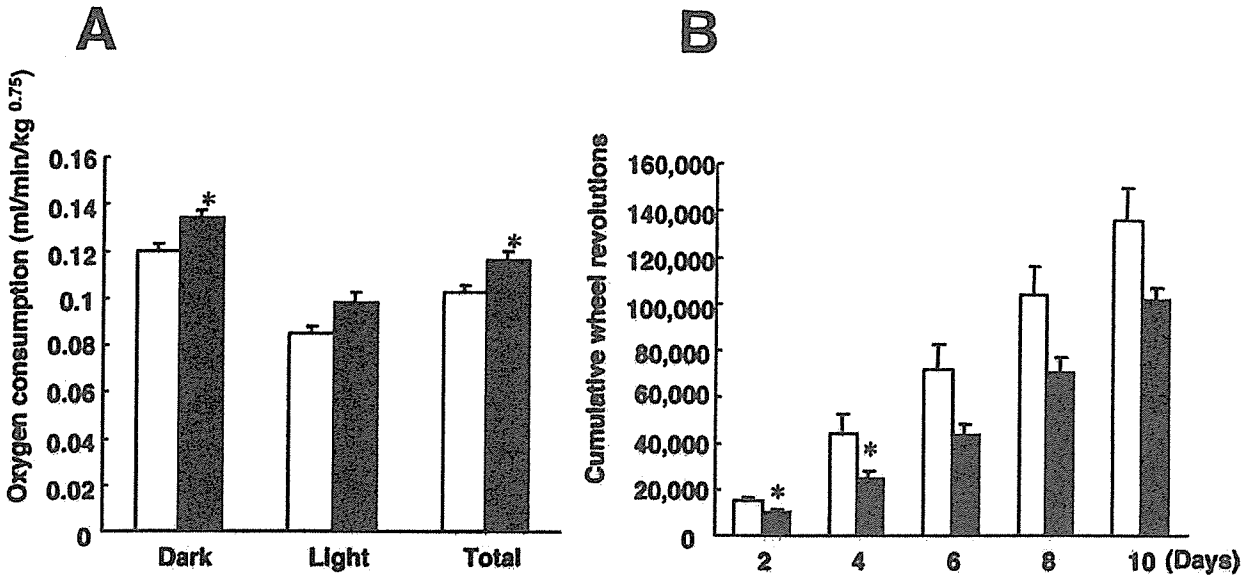

Figure 1. PGC-1α overexpression increases energy expenditure. **A:** Oxygen consumption in PGC-1α mice. Oxygen consumption by 10-week-old female mice housed individually was monitored during the dark cycle (7 p.m. to 7 a.m.) and the light cycle (7 a.m. to 7 p.m.). Each column shows the mean ± SEM values. Open column, wild type; closed column, PGC-1α mice. Wild type, $n = 3$; PGC-1α mice, $n = 6$ (a mixture of three D-line and three E-line mice). $^*P < 0.05$ versus wild-type mice. **B:** Running wheel activities of PGC-1α mice. The number of revolutions was recorded daily for 10 days, and cumulative values are shown. Open column, wild type; closed column, PGC-1α mice. Mice were 8-week-old females. Wild type, $n = 3$; PGC-1α mice, $n = 6$ (a mixture of three D-line and three E-line mice). $^*P < 0.05$ versus wild-type mice.

tion coefficient of 6.2 for NADH.[19] NADH oxidase activity was assayed in 50 mmol/L potassium phosphate buffer (pH 7.7) and 200 μmol/L NADH in the presence or absence of 100 nmol/L antimycin A and 2 mmol/L KCN. The oxidation of NADH was monitored at 340 nm with a mmol/L^{-1} extinction coefficient of 6.2 for NADH.[20] NADH-cytochrome *c* reductase, succinate-cytochrome *c* reductase, ubiquinol-cytochrome *c* reductase, and COX activities were measured as described previously.[17,21] Citrate synthase activity was measured as described previously.[22] Each measurement was performed in three times.

Northern Blot Analysis

Northern blot analysis was performed as described previously.[23]

Southern Blot Analysis

To measure mitochondrial DNA (mtDNA) copy number, cDNA probes for mtDNA-COX II and nuclear genome gene-COX IV were generated as described previously.[6] For each sample, 10 μg of total DNA (containing both genomic and mitochondrial DNAs) from gastrocnemius were digested with *Eco*RI and *Nco*I, separated by electrophoresis on 0.8% agarose gels, and transferred overnight to nylon membranes.[1] Blots were then hybridized to COX II and COX IV probes radiolabeled with ^{32}P-dCTP. The blots were washed, and DNA were quantified with an image analyzer (BAS 1800; Fuji Film, Tokyo, Japan) and expressed as the intensity of phosphostimulated luminescence.

Real-Time Polymerase Chain Reaction (PCR) Analysis

Reactions were performed in the 96-well format with SYBR Green PCR Master Mix and a 7500 real-time PCR system (Applied Biosystems, Foster City, CA) with 3 ng of total genomic DNA as template. As a preliminary experiment, we determined appropriate amounts of DNA for the assay. Copy number of COX II was normalized to those of COX IV and 36B4. 36B4 encodes acidic ribosomal phosphoprotein PO,[24] and the 36B4 cDNA probe is widely used as a control in RNase protection experiments to study regulation of the transcription of several genes by estradiol. Mouse-specific primer pairs were: COX II forward, 5′-CCGACTAAATCAAGCAACAGTAAC-A-3′ and COX II reverse, 5′-AAATTTCAGAGCATTGGC-CATAG-3′; COX IV forward, 5′-CTATGTGTATGGCCCC-ATCC-3′ and COX IV reverse, 5′-AGCGGGCTCTCACT-TCTTC-3′; and 36B4 forward, 5′-GGCCCTGCACTCTC-GCTTTC-3′ and 36B4 reverse, 5′-TGCCAGGACG-CGCTTGT-3′.

Measurement of mtDNA Copy Number

The mtDNA content is the mtDNA copy number normalized to the copy number of a gene contained in the nuclear genome. The mtDNA copy number in PGC-1α transgenic mice was expressed by percentages of those in control wild-type mice with the formula: [(mtDNA in PGC-1α transgenic mice/nuclear genome gene in PGC-1α transgenic mice)/(mtDNA in wild-type mice/nuclear genome gene in wild-type mice)] × 100%. Southern

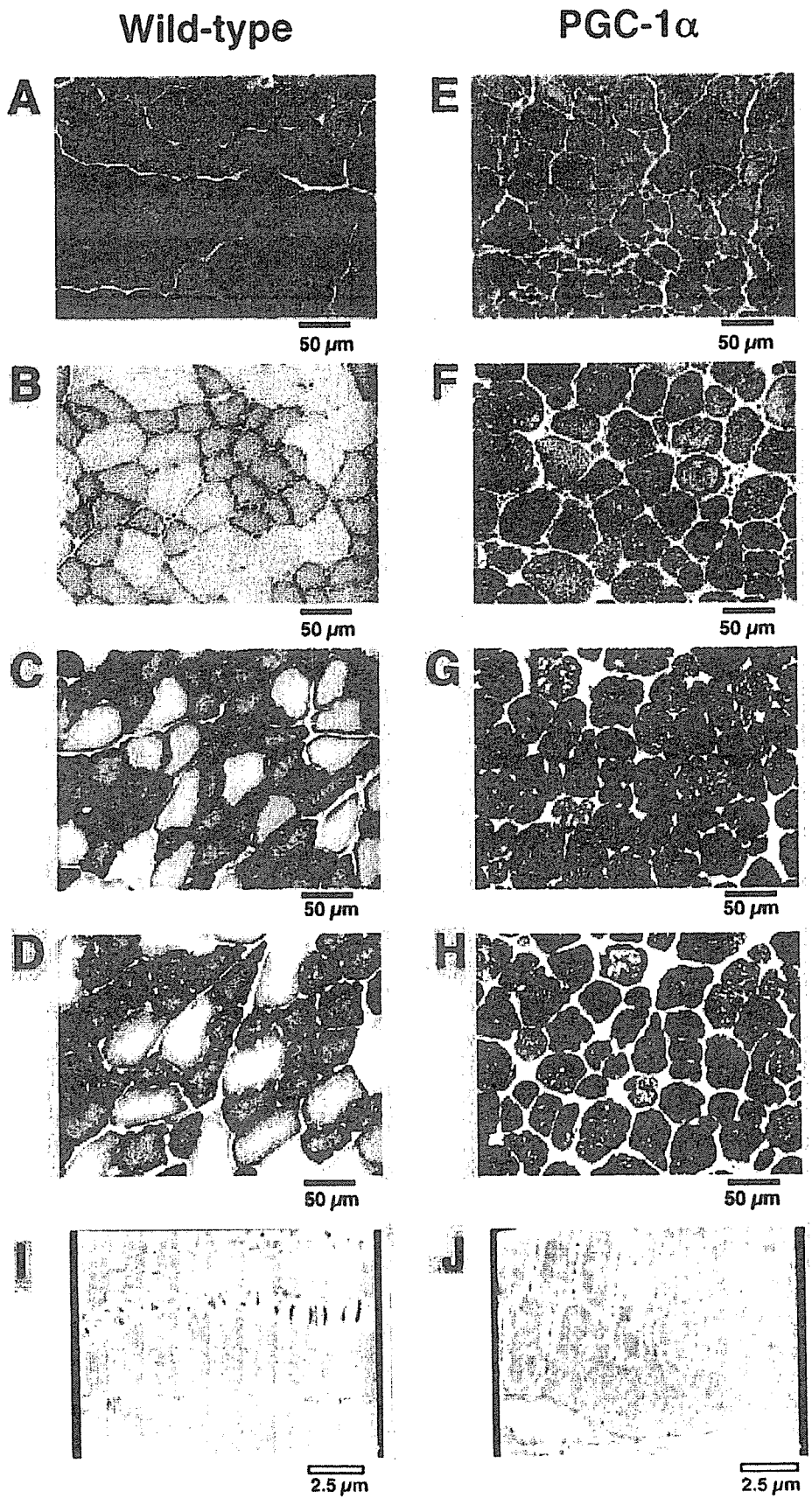
Wild-type
PGC-1α
A
E
50 μm
B
F
50 μm
C
G
50 μm
D
H
50 μm
I
J
2.5 μm

blotting and real-time PCR were used to estimate the copy number of specific genes in skeletal muscles. The mitochondrial gene used for mtDNA copy estimation was COX II, and the copy number of COX II was normalized to the copy number of one of two genes, COX IV or 36B4, contained in the nuclear genome.

Measurements of ATP and AMP Contents

Gastrocnemius was homogenized with 1.0 N perchloric acid and centrifuged at 10,000 × *g* for 15 minutes. After neutralization of the supernatant with calcium carbonate, ATP and AMP concentrations were determined by high performance liquid chromatogram (Phenomenex Luna 5 μ NH_2; mobile phase, sodium phosphate buffer; detector, 260 nm; Torrance, CA).[25,26]

Body Composition Analysis

Mice were anesthetized with pentobarbital sodium, Nembutal (0.08 mg/g body weight; Abbot Laboratories, Chicago, IL), and scanned with a Lunar PIXI mus2 densitometer (Lunar Corp., Madison, WI), equipped for dual-energy X-ray absorptiometry (DEXA).[27]

Statistical Analysis

All data are presented as mean ± SEM. Data from multiple groups were compared by one-way analysis of variance (StatView 5.0; Abacus Concepts, Berkeley, CA). When differences were significant, data were compared between groups by Fisher's protected least significant difference test. Data from two experimental groups were compared by unpaired Student's *t*-test. Statistical significance was defined as $P < 0.05$.

Results

PGC-1α Transgenic Mice Show Increased Energy Expenditure

In our previous study, skeletal muscles of PGC-1α transgenic mice showed the red color characteristic of oxidative muscle and increased levels of enzymes related to mitochondrial oxidative phosphorylation. In the same mice, expression of GLUT4 mRNA was reduced, and the glucose-lowering effects of insulin were impaired.[6] To determine whether PGC-1α transgenic mice show increased energy expenditure, whole-body oxygen consumption was measured in 10-week-old mice (Figure 1A). During both the dark (active) and light (sleeping) phases, PGC-1α transgenic mice showed 1.1-fold higher oxygen consumption than control mice. Because the cumulative number of wheel revolutions was 20% less in PGC-1α transgenic mice (Figure 1B), the increased oxygen consumption in PGC-1α transgenic mice was not attributable to increased voluntary exercise.

Blood triiodothyronine (T3) and thyroxine (T4) concentrations were not altered in 10-week-old PGC-1α transgenic mice. Blood T3 concentrations in wild-type mice, D-line transgenic mice, and E-line transgenic mice were 1.16 ± 0.07 ng/ml, 1.14 ± 0.04 ng/ml, and 1.06 ± 0.01 ng/ml ($n = 3$ each group), respectively. Blood T4 concentrations in wild-type mice, D-line transgenic mice, and E-line transgenic mice were 5.89 ± 0.63 μg/dl, 5.78 ± 0.58 μg/dl, and 5.55 ± 0.29 μg/dl ($n = 3$ each group), respectively.

Numbers of Normal-Sized Mitochondria Were Increased in Skeletal Muscles from PGC-1α Transgenic Mice

We examined whether biogenesis of mitochondria and respiratory chain activity were increased in skeletal muscles from PGC-1α transgenic mice using histochemical staining of tibialis anterior muscle (type 2B-rich fiber muscle) in 16-week-old D-line transgenic mice (Figure 2). H&E staining revealed increased variability in muscle fiber size and increased interstitial cell number and connective tissues in PGC-1α transgenic mice (Figure 2E). Modified Gomori trichrome staining revealed a marked increase in the number of mitochondria in PGC-1α transgenic mice (Figure 2F). In addition, increased COX (Figure 2G) and SDH (Figure 2H) activities in transgenic muscle indicated that the mitochondrial respiratory chain was functional and active. The pathological hallmarks of mtDNA disease, such as ragged-red fibers and COX deficiency,[28] were not observed.

To examine the subcellular structure of myocytes in PGC-1α transgenic mice in detail, extensor digitorum longus skeletal muscle in 16-week-old E-line transgenic mice was examined by electron microscopy (Figure 2J). An increase in the thickness of the *Z*-band that is seen in type-1 fibers and a marked increase in the number of mitochondria in the subsarcolemmal region of muscle fibers were observed. Mitochondrial size was normal, and the alignment of myofibrils was intact in transgenic mice.

To estimate numbers of mitochondria in gastrocnemius from PGC-1α transgenic mice, citrate synthase activity, the most commonly used marker of mitochondrial number,[17] and mtDNA (COX II) copy number relative to those

Figure 2. Morphological analysis of skeletal muscles. Tissue sections from tibialis anterior muscle from 16-week-old wild-type (**A–D**) and PGC-1α transgenic (D-line) mice (**E–H**) are presented. **A** and **E:** H&E staining of tibialis anterior muscle. There are scattered atrophic fibers in PGC-1α transgenic muscle. **B** and **F:** Modified Gomori trichrome staining. An increase in the number of mitochondria was observed in PGC-1α transgenic muscle. **C** and **G:** Staining to detect COX activity. **D** and **H:** Staining to detect SDH activity. Activities of these enzymes were greatly increased in myocytes from PGC-1α transgenic mice. Similar results were obtained with E-line transgenic mice (data not shown). **I** and **J:** Electron microscopy of extensor digitorum longus muscles from wild-type control mice (16 weeks of age) (**I**) and PGC-1α transgenic mice (16 weeks of age, E-line) (**J**). Numbers of mitochondria were markedly higher in transgenic mice, especially in the subsarcolemmal region, than in wild-type mice. Similar results were obtained with D-line transgenic mice (data not shown). Scale bars: 50 μm (**A–H**); 2.5 μm (**I, J**).

Table 1. Estimated Numbers of Mitochondria in Gastrocnemius from 14-Week-Old Mice

	Wild type	PGC-1α/D line	PGC-1α/E line
Citrate synthase activity (μmol/minute/mg protein, %)	0.56 (100)	1.75 (313)	1.66 (296)
COX II/COX IV (%, determined by Southern blot)	100 ± 4 (6)	202 ± 21 (3)‡	165 ± 15 (3)†
COX II/COX IV (%, determined by real-time PCR)	100 ± 5 (6)	178 ± 10 (3)†	214 ± 29 (3)‡
COX II/36B4 (%, determined by real-time PCR)	100 ± 5 (6)	203 ± 8 (3)*	292 ± 58 (3)‡

For measurement of citrate synthase activity, tissues from each group were pooled from three animals before mitochondrial isolation, and the citrate synthase activities of pooled samples were measured. For estimation of mtDNA copy number in skeletal muscle, the relative mtDNA copy number in skeletal muscle from individual mice in each group was calculated as the ratio of COX II (mitochondrial) to COX IV or 36B4 (nuclear) genes as determined by Southern blotting and/or real-time PCR. The relative mtDNA copy number was expressed as the percentage of the ratio in wild type. Numbers of mice were indicated. *$P < 0.05$, †$P < 0.01$, and ‡$P < 0.001$ versus wild-type mice.

of nuclear genome genes (COX IV and 36B4), were measured (Table 1). The copy number of COX IV was estimated by two different methods, Southern blotting and real-time PCR. Citrate synthase activity in PGC-1α transgenic mice was threefold higher than that in wild-type mice. The ratio of COX II copy number to genomic DNA copy number in PGC-1α transgenic mice was twofold to threefold higher than that in wild-type mice, regardless of the detection method or nuclear genome reference gene. These data suggested that if we assume no significant differences in citrate synthase activity and mtDNA copy number in mitochondria between PGC-1α transgenic and wild-type mice, the number of mitochondria in gastrocnemius from PGC-1α transgenic mice was twofold to threefold larger than that in wild-type mice.

Increased Uncoupling of Oxidative Phosphorylation in Skeletal Muscle Mitochondria from PGC-1α Transgenic Mice

To study the function of skeletal muscle mitochondria, we compared the respiration rate (=oxygen consumption) in isolated mitochondria from gastrocnemius and quadriceps of PGC-1α transgenic mice with that in wild-type mice in the absence and presence of oligomycin, an inhibitor of the F_1F_0-ATP synthase.[29] First, the respiration rate of mitochondria was measured under conditions in which mitochondrial substrate and ADP were not limiting to mimic state 3 respiration. To measure uncoupled respiration, oligomycin was added to inhibit oxidative phosphorylation before measurement of respiration rates. In the absence of oligomycin, both lines of PGC-1α transgenic mice showed a twofold to threefold increase of respiration rate on a protein basis of mitochondria-rich fraction (Figure 3A). Because the increased respiration rate observed in PGC-1α transgenic mice was likely attributable to an increased mitochondrial number, we divided the respiration rate by the citrate synthase activity to express respiration rate on a per mitochondrion basis.[17] To normalize the respiration rate to the mitochondrial number, citrate synthase activity rather than mtDNA copy number was used, because the same method for preparation of mitochondria was used for both respiration rate and citrate synthase activity assays. When expressed per unit of citrate synthase activity, the respiration rate was similar between PGC-1α transgenic mice and wild-type mice (Figure 3B), suggesting that respiration was comparable in each mitochondrion in PGC-1α

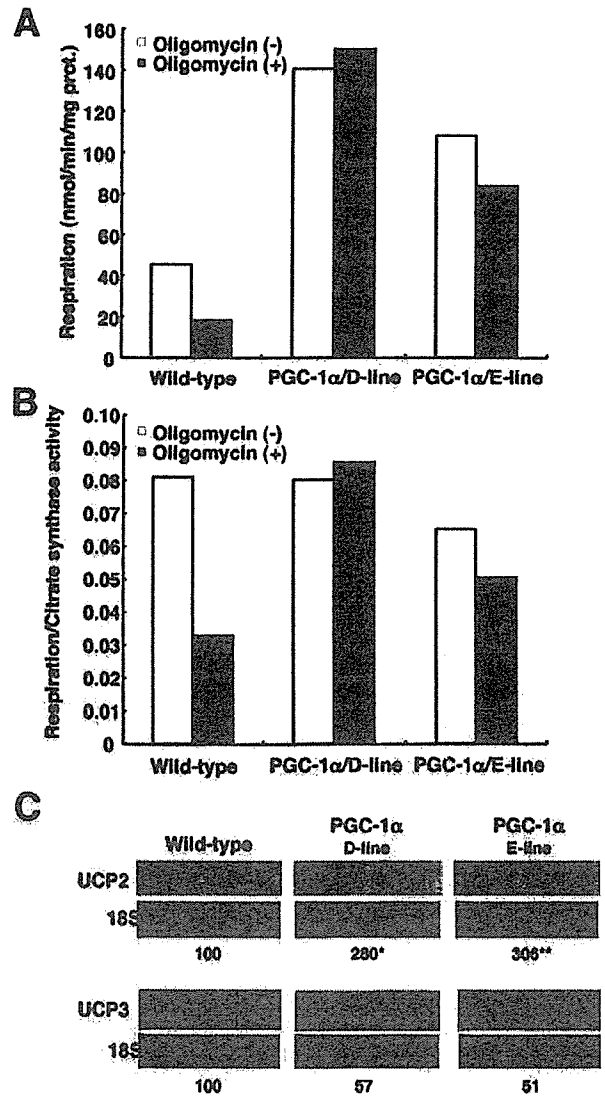

Figure 3. Increased uncoupling of oxidative phosphorylation and UCP2 in skeletal muscle from PGC-1α transgenic mice. Skeletal muscles (gastrocnemius, quadriceps) from both wild-type and PGC-1α male transgenic mice (D-line and E-line) at 14 weeks of age ($n = 3$ each group). Mitochondrial fraction was prepared as described under Materials and Methods. State 3 respiration rate of the mitochondrial fraction was measured in the presence and absence of 2.5 μg/ml oligomycin. Each measurement was performed in triplicate. Each data point is the mean value of the measurements normalized to the protein content (**A**) or to the citrate synthase activity of the fraction (**B**). **C:** Total RNA extracted from gastrocnemius was probed with ^{32}P-labeled human UCP2 and UCP3 cDNA probes. Ribosomal 18S RNA is shown as a loading control. The average densitometric ratios (wild type was set as 100) are under the blot. *$P < 0.05$, **$P < 0.01$ versus wild-type mice.

Table 2. Enzymatic Activity of Respiratory Chain Complexes in Mitochondria from 14-Week-Old Mice

	Enzyme complex (enzyme activity/citrate synthase activity)						
	I	I + III	I + III + IV	II (SDH)	II (SQR)	II + III	IV
Wild type	0.217	0.238	0.279	0.132	0.150	0.177	0.415
PGC-1α/D line	0.201	0.315	0.478	0.102	0.100	0.127	0.868
PGC-1α/E line	0.181	0.225	0.417	0.105	0.099	0.129	0.832

For each group, tissues were pooled from three animals before mitochondrial isolation.

transgenic and wild-type mice. However, the mechanism of respiratory control was different; in wild-type mice, oligomycin-insensitive respiration (=uncoupling) constituted 40% of total respiration, whereas in PGC-1α transgenic mice, most respiration was oligomycin-insensitive. Therefore, PGC-1α transgenic mice contained more mitochondria, but these mitochondria showed lower ATP synthesis (=coupling) and more proton leaks (=uncoupling).

To clarify the mechanism that underlies the increased uncoupling of respiration and ATP synthesis in skeletal muscles of PGC-1α transgenic mice, we measured expression of mRNAs for uncoupling protein UCP1, UCP2, and UCP3. UCP1 mRNA was not expressed in gastrocnemius from PGC-1α transgenic mice. In contrast, expression of UCP2 increased threefold, and that of UCP3 mRNA was decreased slightly (Figure 3C). In liver brown and white adipose tissues, there was no change in levels of UCP1, UCP2, and UCP3 mRNAs (data not shown). Although the role of UCP2 in uncoupling respiration has not been established,[30] the elevated expression of UCP2 might contribute, at least in part, to the uncoupling of respiration observed in PGC-1α transgenic mice.

We then measured the enzymatic activity of respiratory chain complex in mitochondria. Complex I, II, and III had similar activities in PGC-1α transgenic mice and wild-type mice; however, complex IV activity was increased twofold in the transgenic mice when expressed on a per citrate synthase activity basis (=mitochondrial number) (Table 2). An increase in levels of complex IV was confirmed by measurements of COX IV protein, a component of complex IV; COX IV levels in both PGC-1α transgenic mice lines were ~1.5-fold higher than those in wild-type mice, when expressed on a per citrate synthase activity basis (data not shown). Thus, the function of respiratory complexes was not impaired, but the ratio of the complexes was altered in PGC-1α transgenic mice.

ATP Content Was Markedly Decreased in PGC-1α Transgenic Mice

Because mitochondrial respiration in PGC-1α transgenic mice was attributable to proton leak rather than ATP synthesis, we hypothesized that PGC-1α transgenic mice would show reduced ATP levels in their skeletal muscle. To examine ATP levels, we measured the ATP and AMP contents of gastrocnemius (Figure 4). As expected, the ATP concentration in gastrocnemius from both lines of PGC-1α transgenic mice was ~80% lower than that in wild-type mice, whereas the AMP concentration was increased by fivefold to sevenfold. The alteration of the AMP/ATP ratio affects AMP-activated protein kinase (AMPK) activity.[31] Gastrocnemius from PGC-1α transgenic mice showed 4.7-fold higher α1 AMPK activity than control mice, whereas α2 AMPK activity was unchanged (data not shown), confirming that ATP depletion occurred *in vivo*.

PGC-1α Transgenic Mice Develop Skeletal Muscle Atrophy and Adipocyte Proliferation

A marked morphological change was observed in PGC-1α transgenic mice at 25 weeks of age compared with that of mice at 16 weeks of age (Figure 5, B and C). Quadriceps and gastrocnemius muscle (fastest and glycolytic type-2B fiber-rich muscle) from 25-week-old transgenic mice were paler in color than those of wild-type mice (Figure 5, A and C). This change was not observed in soleus muscle (type-1 fiber-rich muscle) (data not shown).

Histological analysis was performed to examine whether the pale, fat-like appearance of the gastrocnemius muscle in transgenic mice was attributable to increased lipid accumulation within myocytes or to an increased adipocyte numbers in skeletal muscles (Figure 5, D–I). Severe muscle atrophy was observed in PGC-1α transgenic mice, and myocytes were replaced by white

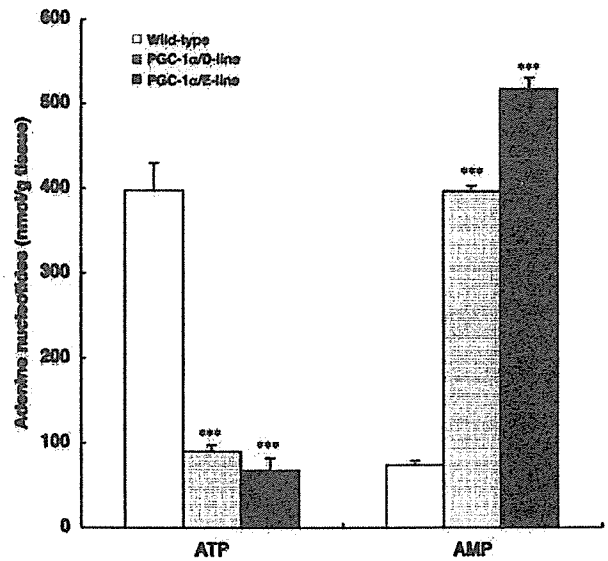

Figure 4. ATP content was markedly decreased in PGC-1α transgenic mice. ATP and AMP contents of gastrocnemius from wild-type, D-line, and E-line transgenic mice were measured at 10 weeks of age. Data are mean ± SEM values ($n = 3$). ***$P < 0.001$ versus wild-type mice.

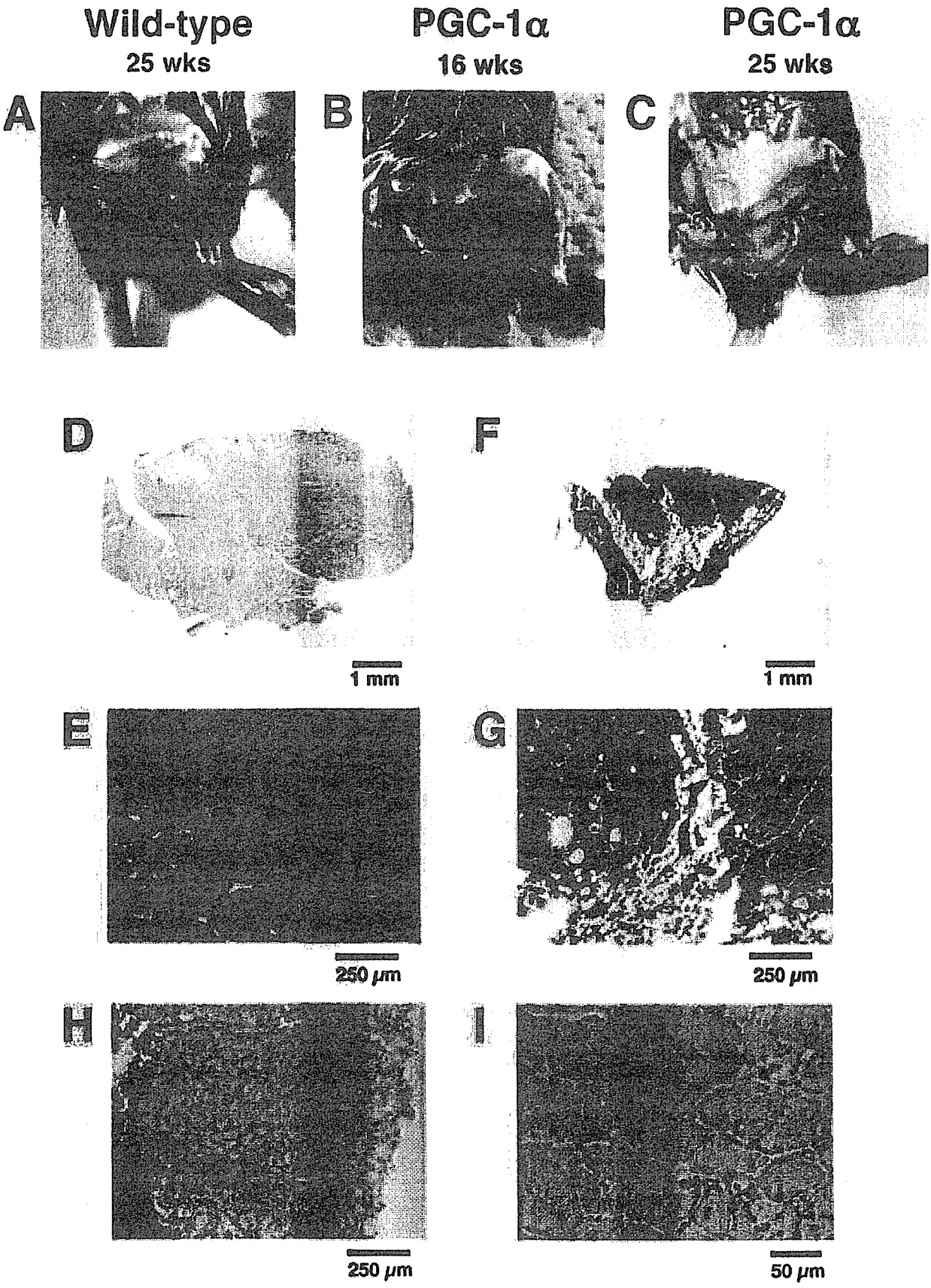
Wild-type
25 wks
PGC-1α
16 wks
PGC-1α
25 wks
A
B
C
D
F
1 mm
1 mm
E
G
250 μm
250 μm
H
I
250 μm
50 μm

Table 3. Physiological Characteristics of 25-Week-Old Wild-Type and PGC-1α Transgenic Male Mice

	Wild type (n = 4)	PGC-1α transgenic (D-line) (n = 3)	PGC-1α transgenic (E-line) (n = 4)
Body weight (g)	41.7 ± 0.6	32.0 ± 3.7*	30.7 ± 1.8†
Body fat (g)	10.4 ± 0.7	6.9 ± 1.1	6.9 ± 0.7*
Body fat (%)	30.4 ± 1.8	26.0 ± 3.7	26.0 ± 1.7
Lean body mass (g)	23.6 ± 0.8	19.4 ± 0.8†	19.5 ± 0.3†
Bone mineral density (g/cm^2)	0.051 ± 0.001	0.046 ± 0.000‡	0.043 ± 0.001‡
White adipose tissue weight (g)			
Epididymal	1.78 ± 0.15	0.88 ± 0.27†	0.66 ± 0.17‡
Retroperitoneal	0.46 ± 0.04	0.38 ± 0.12	0.31 ± 0.09
Subcutaneous	1.64 ± 0.15	0.93 ± 0.29	0.69 ± 0.14*
Brown adipose tissue weight (g)	0.28 ± 0.03	0.13 ± 0.01‡	0.11 ± 0.02‡
Gastrocnemius weight (g)	0.32 ± 0.01	0.17 ± 0.00‡	0.16 ± 0.00‡
Quadriceps weight (g)	0.34 ± 0.01	0.22 ± 0.05*	0.21 ± 0.01†
Liver weight (g)	1.70 ± 0.13	1.17 ± 0.09	1.30 ± 0.05
Spleen weight (g)	0.10 ± 0.00	0.06 ± 0.01	0.08 ± 0.01
Kidney weight (g)	0.48 ± 0.02	0.37 ± 0.02*	0.39 ± 0.01*
Heart weight (g)	0.17 ± 0.01	0.17 ± 0.01	0.17 ± 0.01
Food intake (g/g body weight/day)	0.156 ± 0.014	0.195 ± 0.017	0.192 ± 0.017

*$P < 0.05$, †$P < 0.01$, and ‡$P < 0.001$ versus wild-type mice.

adipose and connective tissues (Figure 5, F and G). Oil red O staining confirmed that the lipid accumulation was attributable not to myocytes but to adipocytes (Figure 5, H and I). Expression of mRNAs typically observed in adipose tissues, such as aP2, HSL, and perilipin, was significantly higher in gastrocnemius from PGC-1α transgenic mice than in gastrocnemius from wild-type mice at 25 weeks of age (data not shown). At 16 weeks of age, increases in the interstitial cell number and amount of connective tissue were observed, but lipid accumulation was absent (Figure 2). These data indicate that, in skeletal muscle tissues from PGC-1α transgenic mice, infiltration of adipocytes occurs rapidly from 4 to 6 months of age, concomitant with the progression of muscle atrophy.

PGC-1α Transgenic Mice Were 25% Smaller than Wild-Type Mice at 25 Weeks of Age

To further characterize PGC-1α transgenic mice, body composition and tissue weights were measured in two independent lines of PGC-1α transgenic mice at 25 weeks of age (Table 3). Although food intake was not different from controls, mean body weight of PGC-1α transgenic mice in both lines was ~25% lower than that of wild-type mice. DEXA scan revealed that both fat mass and lean body mass were decreased in transgenic mice. Bone mineral density was also significantly lower in PGC-1α transgenic mice. The tissue weights of white adipose tissue, brown adipose tissue, skeletal muscles, liver, spleen, and kidney in transgenic mice were 30 to 50% lower than those in wild-type mice. Thus, PGC-1α transgenic mice showed growth retardation with reductions in both lean body mass and fat mass.

Discussion

In the present study, we found that overexpression of PGC-1α in mouse skeletal muscle increased mitochondria numbers and energy expenditure, and eventually caused muscle atrophy, especially of type 2B fiber-rich muscles. PGC-1α transgenic mice showed normal mitochondrial COX and SDH activities (Figure 2, G and H) and normal respiratory chain enzymatic activities (Table 2); however, ATP content was reduced by increased uncoupling.

The marked decrease in the ATP content of type-2B fiber-rich muscles suggests that ATP depletion might be a major cause of muscle atrophy in PGC-1α transgenic mice (Figures 4 and 5). Consistent with our present findings, overexpression of PGC-1α in heart promotes mitochondrial biogenesis but leads to dilated cardiomyopathy.[4] ATP depletion due to impairment of mitochondrial functions is involved in the pathogenesis of a wide variety of inherited and acquired human diseases, including cardiomyopathy, neuromuscular dysfunction, and diabetes mellitus.[32] In skeletal muscles, inherited mitochondrial myopathy is due to mutations of genes encoding enzymes responsible for ATP synthesis in mitochondria.[26] Thus, their mitochondria show impaired mitochondrial respiratory function (=ATP synthesis). These mitochondria are increased in number and size and occasionally show abnormal structures, possibly as adaptation against decreased ATP content.[33] In acquired cases of muscle atrophy, aging-mediated muscle atrophy, namely sarcopenia, was mostly due to loss of type-2 fibers.[34,35] In sarcopenia, an increase in intramuscular adipose tissue was accompanied by a reduction in muscle fibers,[36]

Figure 5. Morphological and histological changes in skeletal muscles at 25 weeks of age. **A–C:** Lateral view of hindlimbs from wild-type (**A:** 25 weeks of age) and E-line transgenic (**B:** 16 weeks of age, **C:** 25 weeks of age) mice. Morphological differences were not observed in wild-type muscle between 16 and 25 weeks of age (data not shown). **D–G:** H&E staining of tissue sections from gastrocnemius of wild-type (**D, E**) and E-line transgenic mice (**F, G**). Specimens from transgenic mice showed atrophy of myocytes and increased adipose and interstitial connective tissues. **H** and **I:** Oil red O staining of tissue sections from gastrocnemius of E-line transgenic mice (**H, I**). Staining of lipid was observed in adipose tissue that surrounded the atrophic myocytes (**H**). No positive staining was observed inside the muscle fiber (**I**). Similar results were obtained for D-line transgenic mice (data not shown).

as was observed in our PGC-1α transgenic mice. *In vivo* proton magnetic resonance spectroscopy studies revealed that the mitochondrial ATP synthesis rate in skeletal muscle from elderly people was 46% lower than that in muscles from young patients.[37] Isolated mitochondria from elderly participants showed decreased state 3 (activated) mitochondrial respiration.[38] Taken together, these data indicate that ATP depletion caused by mitochondrial dysfunction might be a cause of sarcopenia. Therefore, ATP depletion in skeletal muscle might be a common feature of muscle atrophy.

However, reported clinical cases of ATP depletion attributable to increased uncoupling of respiration are very rare. Uncoupling-mediated muscle atrophy in humans was first described by Luft and colleagues[8,9] in 1959 and was called Luft's disease. This disease is important not only because it was the first identified human mitochondrial disorder but also because Luft's disease is still the only mitochondrial disease caused by uncoupling of oxidative phosphorylation. The cause of Luft disease is unknown because this disease is extremely rare; only one patient has been reported by DiMauro and colleagues[10] and in addition to the original case described by Luft and colleagues. To date, no animal model has been available. Patients with Luft's disease show increased energy expenditure and reduced body weight; however, thyroid hormone levels are normal. PGC-1α transgenic mice also exhibit these cardinal features with biochemical evidence of uncoupling of oxidative phosphorylation. Therefore, our mice recapitulate the phenotype of Luft's disease, although there is some difference in mitochondrial morphology. Mitochondria in Luft's disease were highly variable in size and shape with a range of abnormal internal structures, including densely packed cristae, tubular structures, electron-dense regularly layered cores, and concentric structures.[9,10,39] In PGC-1α transgenic mice, such morphological abnormalities in mitochondria were not observed. The reasons for these differences are unknown. The mechanism that underlies increased uncoupling of respiration by PGC-1α overexpression is also not clear. Increased expression of UCP2 may partially contribute to uncoupling (Figure 3C), but other unknown uncoupling proteins might also be involved.

The hypothesis that ATP depletion induces muscle atrophy may be supported by the fact that overexpression of UCP1 in skeletal muscle also reduces the masses of type-2B fiber-rich muscles (gastrocnemius and plantaris), which are vulnerable to ATP depletion, but not those of heart and soleus muscle, which undergo constant repeated contractions with high ATP supply.[40] Similar phenotype of mice overexpressing UCP1, the soleus muscle in PGC-1α transgenic mice is not atrophic, suggesting a close relation between ATP content and muscle mass. In fact, after exercise training, the number of functional mitochondria and glucose and fatty acid oxidation are increased in skeletal muscle, possibly because of an increase of PGC-1α; however, muscle weight is increased.[41] Thus, when myocyte energy expenditure is increased, a large supply of substrate from blood fatty acids and glucose might be required for maintenance of skeletal muscle integrity. Thus, mismatch between energy demand and supply may precipitate organ dysfunction.

Although the respiratory functions of complexes I, II, III, and IV in PGC-1α transgenic mice were not impaired, the activity of complex IV activity was much higher than those of complexes I, II, and III (Table 2). Conversely, in humans, a significant age-related decline in COX activity (complex IV of the respiratory chain) has been observed, but SDH activity (complex II of the respiratory chain) is not altered.[42] These data further indicate that aging might reduce PGC-1α activity in skeletal muscle. It is not clear why complex IV was preferentially activated by PGC-1α overexpression. Complexes I, II, and III are the significant sources of reactive oxygen species, namely superoxide and hydrogen peroxide, whereas complex IV is not.[43] We observed increased superoxide anion production in mitochondria from PGC-1α transgenic mice, when isolated mitochondria were incubated with either NADH (twofold increase per mg protein) or succinate (fourfold increase per mg protein) (data not shown). To prevent harmful increases in reactive oxygen species, adaptive mechanisms might suppress increases in expression of complexes I, II, and III in transgenic mice.

In this study, we demonstrated that overexpression of PGC-1α increased uncoupled oxidative phosphorylation and caused ATP deprivation, resulting in muscle atrophy, the phenotype of the first human mitochondrial disease described by Luft and colleagues,[8,9] more than 50 years ago. This mouse model confirms Luft's historical observation that uncoupling of oxidative phosphorylation causes myopathy. Furthermore, our results suggest that the genetic cause of Luft's disease may be a defect in the PGC-1α-related pathway. However, this is impossible to confirm until a new case can be found. Development of a mouse model of Luft's disease prompts further studies to understand the molecular mechanisms by which uncoupled oxidative phosphorylation leads to muscle atrophy.

Acknowledgments

We thank Dr. Ikuya Nonaka and Dr. Yu-ichi Goto at the National Center of Neurology and Psychiatry (Tokyo) for advice on mitochondrial myopathy and Dr. Constantine Londos at the National Institutes of Health (Bethesda, MD) for providing perilipin cDNA.

References

1. Puigserver P, Wu Z, Park CW, Graves R, Wright M, Spiegelman BM: A cold-inducible coactivator of nuclear receptors linked to adaptive thermogenesis. Cell 1998, 92:829–839
2. Wu Z, Puigserver P, Andersson U, Zhang C, Adelmant G, Mootha V, Troy A, Cinti S, Lowell B, Scarpulla RC, Spiegeman BM: Mechanisms controlling mitochondrial biogenesis and respiration through the thermogenic coactivator PGC-1. Cell 1999, 98:115–124
3. Vega RB, Huss JM, Kelly DP: The coactivator PGC-1 cooperates with peroxisome proliferator-activated receptor alpha in transcriptional control of nuclear genes encoding mitochondrial fatty acid oxidation enzymes. Mol Cell Biol 2000, 20:1868–1876
4. Lehman JJ, Barger PM, Kovacs A, Saffitz JE, Medeiros DM, Kelly DP: Peroxisome proliferator-activated receptor gamma coactivator-1 pro-

motes cardiac mitochondrial biogenesis. J Clin Invest 2000, 106:847–856
5. Lin J, Wu H, Tarr PT, Zhang CY, Wu Z, Boss O, Michael LF, Puigserver P, Isotani E, Olson EN, Lowell BB, Bassel-Duby R, Spiegelman BM: Transcriptional co-activator PGC-1 alpha drives the formation of slow-twitch muscle fibres. Nature 2002, 418:797–801
6. Miura S, Kai Y, Ono M, Ezaki O: Overexpression of peroxisome proliferator-activated receptor gamma coactivator-1alpha down-regulates GLUT4 mRNA in skeletal muscles. J Biol Chem 2003, 278:31385–31390
7. St.-Pierre J, Lin J, Krauss S, Tarr PT, Yang R, Newgard CB, Spiegelman BM: Bioenergetic analysis of peroxisome proliferator-activated receptor gamma coactivators 1alpha and 1beta (PGC-1alpha and PGC-1beta) in muscle cells. J Biol Chem 2003, 278:26597–26603
8. Ernster L, Ikkos D, Luft R: Enzymic activities of human skeletal muscle mitochondria: a tool in clinical metabolic research. Nature 1959, 184:1851–1854
9. Luft R, Ikkos D, Palmieri G, Ernster L, Afzelius B: A case of severe hypermetabolism of nonthyroid origin with a defect in the maintenance of mitochondrial respiratory control: a correlated clinical, biochemical, and morphological study. J Clin Invest 1962, 41:1776–1804
10. DiMauro S, Bonilla E, Lee CP, Schotland DL, Scarpa A, Conn Jr H, Chance B: Luft's disease. Further biochemical and ultrastructural studies of skeletal muscle in the second case. J Neurol Sci 1976, 27:217–232
11. Tsuboyama-Kasaoka N, Takahashi M, Tanemura K, Kim HJ, Tange T, Okuyama H, Kasai M, Ikemoto S, Ezaki O: Conjugated linoleic acid supplementation reduces adipose tissue by apoptosis and develops lipodystrophy in mice. Diabetes 2000, 49:1534–1542
12. Black JT, Judge D, Demers L, Gordon S: Ragged-red fibers. A biochemical and morphological study. J Neurol Sci 1975, 26:479–488
13. Seligman AM, Karnovsky MJ, Wasserkrug HL, Hanker JS: Nondroplet ultrastructural demonstration of cytochrome oxidase activity with a polymerizing osmiophilic reagent, diaminobenzidine (DAB). J Cell Biol 1968, 38:1–14
14. Dubowitz V, Brooke M: A Modern Approach, Muscle Biopsy. London, Saunders, 1973
15. Pallotti F, Lenaz G: Isolation and subfractionation of mitochondria from animal cells and tissue culture lines. Methods Cell Biol 2001, 65:1–35
16. Lowry OH, Rosebrough NJ, Farr AL, Randall RJ: Protein measurement with the Folin phenol reagent. J Biol Chem 1951, 193:265–275
17. Trounce IA, Kim YL, Jun AS, Wallace DC: Assessment of mitochondrial oxidative phosphorylation in patient muscle biopsies, lymphoblasts, and transmitochondrial cell lines. Methods Enzymol 1996, 264:484–509
18. Kita K, Vibat CR, Meinhardt S, Guest JR, Gennis RB: One-step purification from Escherichia coli of complex II (succinate: ubiquinone oxidoreductase) associated with succinate-reducible cytochrome b556. J Biol Chem 1989, 264:2672–2677
19. Miyadera H, Amino H, Hiraishi A, Taka H, Murayama K, Miyoshi H, Sakamoto K, Ishii N, Hekimi S, Kita K: Altered quinone biosynthesis in the long-lived clk-1 mutants of Caenorhabditis elegans. J Biol Chem 2001, 276:7713–7716
20. Ventura B, Genova ML, Bovina C, Formiggini G, Lenaz G: Control of oxidative phosphorylation by complex I in rat liver mitochondria: implications for aging. Biochim Biophys Acta 2002, 1553:249–260
21. Birch-Machin MA, Turnbull DM: Assaying mitochondrial respiratory complex activity in mitochondria isolated from human cells and tissues. Methods Cell Biol 2001, 65:97–117
22. Srere PA: Citrate synthase. Methods Enzymol 1969, 13:3–11
23. Tsuboyama-Kasaoka N, Tsunoda N, Maruyama K, Takahashi M, Kim H, Ikemoto S, Ezaki O: Up-regulation of uncoupling protein 3 (UCP3) mRNA by exercise training and down-regulation of UCP3 by denervation in skeletal muscles. Biochem Biophys Res Commun 1998, 247:498–503
24. Laborda J: 36B4 cDNA used as an estradiol-independent mRNA control is the cDNA for human acidic ribosomal phosphoprotein PO. Nucleic Acids Res 1991, 19:3998
25. Watanabe A, Tsuneishi E, Takimoto Y: Analysis of ATP and its breakdown products in beef by reversed-phase HPLC. J Food Sci 1989, 54:1169–1172
26. Scott MD, Baudendistel LJ, Dahms TE: Rapid separation of creatine, phosphocreatine and adenosine metabolites by ion-pair reversed-phase high-performance liquid chromatography in plasma and cardiac tissue. J Chromatogr 1992, 576:149–154
27. Nagy TR, Clair AL: Precision and accuracy of dual-energy X-ray absorptiometry for determining in vivo body composition of mice. Obes Res 2000, 8:392–398
28. Larsson NG, Clayton DA: Molecular genetic aspects of human mitochondrial disorders. Annu Rev Genet 1995, 29:151–178
29. Brand M: Mitochondria: A Practical Approach. Edited by G Brown, C Cooper Oxford University Press, 1995, pp 39–62
30. Esteves TC, Brand MD: The reactions catalysed by the mitochondrial uncoupling proteins UCP2 and UCP3. Biochim Biophys Acta 2005, 1709:35–44
31. Hardie DG, Carling D, Carlson M: The AMP-activated/SNF1 protein kinase subfamily: metabolic sensors of the eukaryotic cell? Annu Rev Biochem 1998, 67:821–855
32. Wallace DC: Mitochondrial diseases in man and mouse. Science 1999, 283:1482–1488
33. Heddi A, Lestienne P, Wallace DC, Stepien G: Mitochondrial DNA expression in mitochondrial myopathies and coordinated expression of nuclear genes involved in ATP production. J Biol Chem 1993, 268:12156–12163
34. Larsson L, Sjodin B, Karlsson J: Histochemical and biochemical changes in human skeletal muscle with age in sedentary males, age 22–65 years. Acta Physiol Scand 1978, 103:31–39
35. Tomonaga M: Histochemical and ultrastructural changes in senile human skeletal muscle. Am Geriatr Soc 1977, 25:125–131
36. Song MY, Ruts E, Kim J, Janumala I, Heymsfield S, Gallagher D: Sarcopenia and increased adipose tissue infiltration of muscle in elderly African American women. Am J Clin Nutr 2004, 79:874–880
37. Petersen KF, Befroy D, Dufour S, Dziura J, Ariyan C, Rothman DL, DiPietro L, Cline GW, Shulman GI: Mitochondrial dysfunction in the elderly: possible role in insulin resistance. Science 2003, 300:1140–1142
38. Trounce I, Byrne E, Marzuki S: Decline in skeletal muscle mitochondrial respiratory chain function: possible factor in ageing. Lancet 1989, 1:637–639
39. Sjostrand FS: Molecular pathology of Luft disease and structure and function of mitochondria. J Submicrosc Cytol Pathol 1999, 31:41–50
40. Couplan E, Gelly C, Goubern M, Fleury C, Quesson B, Silberberg M, Thiaudiere E, Mateo P, Lonchampt M, Levens N, De Montrion C, Ortmann S, Klaus S, Gonzalez-Barroso MD, Cassard-Doulcier AM, Ricquier D, Bigard AX, Diolez P, Bouillaud F: High level of uncoupling protein 1 expression in muscle of transgenic mice selectively affects muscles at rest and decreases their IIb fiber content. J Biol Chem 2002, 45:43079–43088
41. Holloszy JO, Kohrt WM, Hansen PA: The regulation of carbohydrate and fat metabolism during and after exercise. Front Biosci 1998, 3:D1011–D1027
42. Müller-Höcker J: Cytochrome c oxidase deficient fibres in the limb muscle and diaphragm of man without muscular disease: an aged-related alteration. J Neurol Sci 1990, 100:14–21
43. Jezek P, Hlavatá L: Mitochondria in homeostasis of reactive oxygen species in cell, tissue, and organism. Int J Biochem Cell Biol 2005, 37:2478–2503

Available online at www.sciencedirect.com
SCIENCE DIRECT
ELSEVIER
Immunology Letters 106 (2006) 82–90
Immunology Letters
www.elsevier.com/locate/

Modulation of acute graft-versus-host disease and chimerism after adoptive transfer of *in vitro*-expanded invariant Vα14 natural killer T cells

Masaki Kuwatani [a,b], Yoshinori Ikarashi [a,*], Akira Iizuka [a,d], Chihiro Kawakami [a], Gary Quinn [c], Yuji Heike [a], Mitsuzi Yoshida [a], Masahiro Asaka [b], Yoichi Takaue [d], Hiro Wakasugi [a,*]

[a] *Pharmacology Division, National Cancer Center Research Institute, 5-1-1 Tsukiji, Chuo-ku, Tokyo 104-0045, Japan*
[b] *Department of Gastroenterology, Graduate School of Medicine, Hokkaido University, Sapporo 060-8638, Japan*
[c] *Section for Studies on Metastasis, National Cancer Center Research Institute, 5-1-1 Tsukiji, Chuo-ku, Tokyo 104-0045, Japan*
[d] *Hematopoietic Stem Cell Transplantation/Immunotherapy Unit, National Cancer Center Hospital, Tokyo, Japan*

Received 22 February 2006; received in revised form 1 May 2006; accepted 3 May 2006
Available online 23 May 2006

Abstract

Mouse natural killer T cells with an invariant Vα14-Jα18 TCR rearrangement (Vα14i NKT cells) are able to regulate immune responses through rapid and large amounts of Th1 and Th2 cytokine production. It has been reported that *in vivo* administration of the Vα14i NKT cell ligand, α-galactosylceramide (α-GalCer) significantly reduced morbidity and mortality of acute graft-versus-host disease (GVHD) in mice. In this study, we examined whether adoptive transfer of *in vitro*-expanded Vα14i NKT cells using α-GalCer and IL-2 could modulate acute GVHD in the transplantation of spleen cells of C57BL/6 mice into (B6 × DBA/2) F_1 mice.

We found that the adoptive transfer of cultured spleen cells with a combination of α-GalCer and IL-2, which contained many Vα14i NKT cells, modulated acute GVHD by exhibiting long-term mixed chimerism and reducing liver damage. Subsequently, the transfer of Vα14i NKT cells purified from spleen cells cultured with α-GalCer and IL-2 also inhibited acute GVHD. This inhibition of acute GVHD by Vα14i NKT cells was blocked by anti-IL-4 but not by anti-IFN-γ monoclonal antibody. Therefore, the inhibition was dependent on IL-4 production by Vα14i NKT cells. Our findings highlight the therapeutic potential of *in vitro*-expanded Vα14i NKT cells for the prevention of acute GVHD after allogeneic hematopoietic stem cell transplantation.

Keywords: Graft-versus-host disease; NKT cell; α-Galactosylceramide; Chimerism

1. Introduction

Mouse natural killer T cells with an invariant Vα14-Jα18 TCR rearrangement (Vα14i NKT cells) are a unique T cell population that is specifically activated by a synthetic glycolipid, α-galactosylceramide (α-GalCer) in a non-classical MHC class I molecule CD1d-restricted manner [1]. Vα14i NKT cells are known as immunomodulating cells influencing the Th1/Th2 balance, mainly via rapid secretion of robust amounts of Th1 (such as IFN-γ) and Th2 (IL-4, IL-10 and IL-13) cytokines. Thus, Vα14i NKT cells have a critical role for various immune responses including autoimmune disease [2], tumor-immunity [3,4], infection and allogeneic transplantation [5].

Graft-versus-host disease (GVHD) is an intractable and severe obstacle in allogeneic hematopoietic stem cell transplantation (HSCT). To resolve this, various treatments such as donor T cell depletion [6] and immunosuppressive drugs [7] have been attempted. In mouse acute GVHD models, a Th1 dominant cytokine secretion profile and expansion of donor $CD8^+$ T cells have been reported [8–10]. Hence it is suggested that acute GVHD is reduced by the skewed Th2 polarization of host immunity and the suppression of donor $CD8^+$ T cell

Abbreviations: GVHD, graft-versus-host disease; HSCT, hematopoietic stem cell transplantation; α-GalCer, α-galactosylceramide; Vα14i NKT cells, natural killer T cells with an invariant Vα14-Jα18 TCR rearrangement; B6, C57BL/6; BDF_1, (B6 × DBA/2) F_1; SC, spleen cells; α-GCSC, SC were cultured with IL-2 and α-GalCer; mAb, monoclonal antibody; Vα24i NKT cells, NKT cells with an invariant Vα24-JαQ TCR rearrangement; GOT, glutamic oxaloacetic transaminase; GPT, glutamic pyruvic transaminase

* Corresponding authors. Tel.: +81 3 3547 5248; fax: +81 3 3542 1886.
E-mail addresses: yikarash@gan2.ncc.go.jp (Y. Ikarashi), hwakasug@gan2.ncc.go.jp (H. Wakasugi).

0165-2478/$ – see front matter © 2006 Elsevier B.V. All rights reserved.
doi:10.1016/j.imlet.2006.05.001

expansion. It has been reported that immune-regulatory cells such as $CD4^+$ $CD25^+$ T cell [11], $NK1.1^+$ or $DX5^+$ T cells [5,12] reduced acute GVHD. Recently, it has been demonstrated that the administration of α-GalCer to induce IL-4 production by host Vα14i NKT cells suppressed acute GVHD in a mouse model [13,14], which suggests the potential of α-GalCer/NKT cell-based immunotherapy for the prevention of acute GVHD. Nevertheless, the frequency of human NKT cells with an invariant Vα24-JαQ TCR rearrangement paired with Vβ11 TCR (Vα24i NKT cells) is very low (less than 0.5%) in peripheral blood mononuclear cells [15]. Furthermore, it has been reported that the number of NKT cells in recipients of HSCT with acute GVHD is lower compared to those without acute GVHD [16]. Given that *in vivo* administration of α-GalCer could not expand host NKT cells in some cases [17,18], we hypothesized that an adoptive transfer of *in vitro*-expanded NKT cells would be more effective than *in vivo* administration of α-GalCer alone in patients with acute GVHD.

Several investigators have reported that human Vα24i NKT cells were effectively expanded using α-GalCer plus a combination of cytokines, such as IL-2, IL-7 and IL-15 *in vitro* [19–22], while mouse Vα14i NKT cells could also be expanded with α-GalCer *in vitro* [1,23]. We found that the culture of spleen cells with α-GalCer and IL-2 for 4 days efficiently induced the expansion of Vα14i NKT cells [24]. Moreover, we revealed that *in vitro*-expanded Vα14i NKT cells retained the ability to produce IL-4 and IFN-γ and migrated into peripheral organs after adoptive transfer [24]. Therefore, adoptive transfer of *in vitro*-expanded Vα14i NKT cells may reduce acute GVHD.

In this study, we demonstrated that adoptive transfer of *in vitro*-expanded Vα14i NKT cells reduced acute GVHD such as liver injury and maintained long-term mixed chimerism. This effect is dependent on IL-4 using neutralizing anti-IL-4 monoclonal antibody. Our findings indicate the therapeutic potential of *in vitro*-expanded Vα14i NKT cells for the prevention of acute GVHD.

2. Materials and methods

2.1. Mice

Female C57BL/6N (B6, H-2^b), DBA/2N (DBA/2, H-2^d) and (C57BL/6 × DBA/2) F_1 (BDF_1, H-$2^{b/d}$) mice were purchased from Charles River Japan (Kanagawa, Japan). All mice maintained in our animal facilities were 8–12 weeks of age at the time of transplantation. All animal protocols for this study were reviewed and approved by the committee for ethics of animal experimentation in the National Cancer Center.

2.2. Monoclonal antibodies and reagents

Fluorescein isothiocyanate (FITC)-conjugated mAb against H-$2K^d$ and phycoerythrin (PE)-conjugated mAb against CD3, CD4, CD8, B220, DX-5, NK1.1 were all purchased from BD Pharmingen (San Diego, CA). For blocking IL-4 and IFN-γ *in vivo*, anti-IL-4 (clone: 11B11) and anti-IFN-γ (clone: R4-6A2) mAb were obtained from the ascites of nude mice inoculated with the hybridomas. α-GalCer was kindly provided by Pharmaceutical Research Laboratory, KIRIN Brewery Co. Ltd. (Gunma, Japan). Recombinant human IL-2 was kindly donated by Takeda Chemical Ind. Ltd. (Osaka, Japan). PE or APC-conjugated CD1d/α-GalCer tetramer was prepared in a baculovirus expression system as previously described [25]. Mouse CD1d/β2-microglobulin expression vector was provided by Dr. M. Kronenberg (La Jolla Institute for Allergy and Immunology, San Diego, CA).

2.3. Cell culture and purification of Vα14i NKT cells

In vitro expansion of Vα14i NKT cells was performed as previously described [24]. Briefly, spleen cell (SC) suspensions (5×10^5 cells/ml) were cultured with α-GalCer (50 ng/ml) and recombinant human IL-2 (100 IU/ml) in RPMI 1640 culture medium (Sigma–Aldrich, Saint Louis, MO) supplemented with 8% fetal calf serum (JRH Biosciences, Lenexa, KS), penicillin (50 U/ml), streptomycin (50 μg/ml) and 2-mercaptoethanol (5×10^{-5} M) for 4 days in a 37 °C, 5% CO_2 incubator. In some experiments, *in vitro*-expanded Vα14i NKT cells were positively selected with PE-conjugated CD1d/α-GalCer tetramer, anti-PE microbeads and SuperMACS system (Miltenyi Biotec, Bergisch Gladbach, Germany), as preciously described [24]. In brief, dead cells were removed from cultured SC as described above using a dead cell removal kit (Miltenyi Biotec), LS column (Miltenyi Biotec) and SuperMACS system (Miltenyi Biotec). Then, the SC were preincubated with anti-CD16/32 (2.4G2, BD PharMingen), stained with appropriate diluted PE-conjugated CD1d/α-GalCer tetramer on ice in the dark for 30 min, and washed three times by buffer (phosphate buffered saline supplemented with 0.5% bovine serum albumin and 2 mM EDTA). The stained cells were then incubated with anti-PE microbeads (Miltenyi Biotec) (1×10^7 cells/microbeads in 40 μl) on ice in the dark for 30 min, suspended in 2 ml buffer, and finally passed through a LS column using the SuperMACS system with additive 3× 3 ml of buffer for washing column. Consequently, we acquired the purified Vα14i NKT cells as residual cells in the column. The purity of CD1d/α-GalCer $tetramer^+$ $CD3^+$ cells was more than 96%.

2.4. Cell transfer and treatment with antibodies

For the induction of GVHD, 7×10^7 spleen cells from B6 mice were transferred into BDF_1 mice intravenously through the tail vein (GVHD mice) as previously described [8]. One day later, 2×10^7 spleen cells cultured with α-GalCer and IL-2 for 4 days (α-GCSC) were injected intravenously into BDF_1 mice with GVHD. In other experiments, purified Vα14i NKT cells were transferred into GVHD mice. In some experiments, GVHD mice were administered with anti-IL-4 mAb (3 mg/mouse) or anti-IFN-γ mAb (1 mg/mouse) intraperitoneally on the day of α-GCSC transfer, referring previous reports for effective doses of mAbs [26–28].

2.5. Flow cytometry

The phenotype of cells was determined by multicolor flow cytometery as previously described [24]. To prevent non-specific binding of mAb, cells were pre-incubated with anti-CD16/32 (2.4G2, BD PharMingen). The relative percentages of host- and donor-origin cells in the recipient spleens were determined by anti-H2-K^d (recipient type) as an indicator of GVHD in which donor chimerism was elevated [29]. The relative percentage of donor-origin cells (% donor chimerism) in chimeric recipients was calculated by the following formula: 100 − %H-2K^d positive cells.

In addition, for the determination of a lineage-specific chimerism, recipient spleens were stained with FITC-conjugated antibody against H-2K^d and PE-conjugated antibodies against CD3, CD4, CD8, B220, DX-5. Vα14i NKT cell frequency was determined by FITC-conjugated CD3 and APC-conjugated CD1d/α-GalCer tetramer. Propidium iodide was used to exclude dead cells. The stained cells were analyzed using FACSCalibur (BD Biosciences, San Jose, CA) and Flow Jo software (Tree Star Inc., San Carlos, CA).

2.6. Assessment of GVHD

Recipient mice were sacrificed on day 14. The serum glutamic oxaloacetic transaminase (GOT) and glutamic pyruvic transaminase (GPT) levels were detected (SRL Inc., Tokyo, Japan) by serological examination using standard methodologies. Additionally, liver and small bowel were embedded in paraffin, cut into 5 μm-thick sections, and stained with H&E for histological examination.

3. Results

3.1. Adoptive transfer of spleen cells cultured with α-GalCer and IL-2 (α-GCSC) inhibit donor T cell engraftment in mice with acute GVHD.

In order to obtain a large number of Vα14i NKT cells, spleen cells from BDF_1 mice were cultured with α-GalCer and IL-2 for 4 days as previously reported [24]. As shown in Fig. 1A, the percentage of $CD3^+$ CD1d/α-GalCer $tetramer^+$ cells increased approximately 20-fold after expansion in culture. In

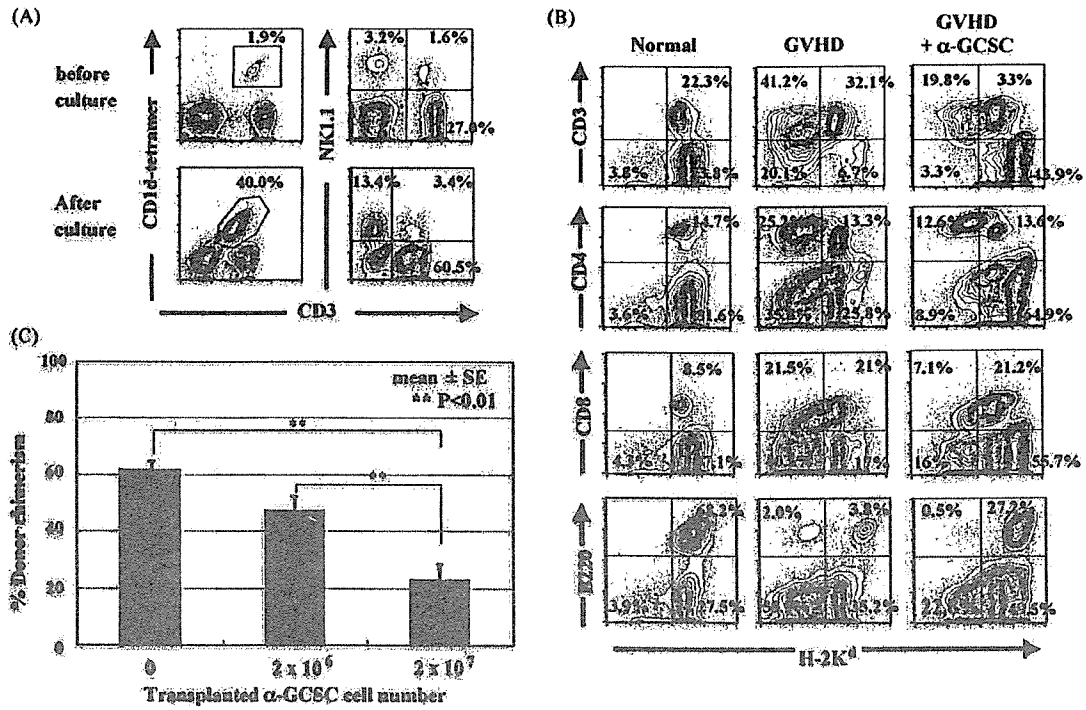

Fig. 1. Adoptive transfer of spleen cells cultured with α-GalCer and IL-2 reduced percentages of donor chimerism depending on cell number. (A) Spleen cells (SC) of BDF_1 mice were cultured with 50 ng/ml α-GalCer and 100 IU/ml IL-2 for 4 days. The percentage of Vα14i NKT cells and $NK1.1^+$ $CD3^-$ NK cells were determined. Before and after culture cells were stained with anti-CD3-FITC, anti-NK1.1-PE mAb and CD1d/α-GalCer tetramer-APC. The numbers in each of the quadrants represent the percentage of total analyzed cells. The fluorescence profiles are representative of at least three independent experiments. (B, C) BDF_1 mice were transferred with 7×10^7 B6 SC on day 0 for GVHD induction and with or without α-GCSC as indicated at 2×10^7 or 2×10^6 on day 1 and then donor chimerism and surface phenotype of SC were analyzed by flow cytometory on day 14. (B) SC of untreated (normal: left column), transplanted with B6 SC alone (GVHD: center column) and transplanted with both B6 SC and 2×10^7 α-GCSC (GVHD + α-GCSC: right column) mice were stained with anti-H-2K^d-FITC and each of anti-CD3, CD4, CD8, B220, DX-5-PE mAb at day 14. The numbers in each of the quadrants represent the percentage of total analyzed cells. The fluorescence profiles are representative of at least three independent experiments. (C) The bars indicate averages of percentage of donor chimerism with standard error of the mean. The number of each group is α-GCSC transfer of 0: $n=6$; 2×10^6: $n=6$; 2×10^7: $n=7$. $^{**}p<0.01$ versus group of α-GCSC transfer of 0. The differences between groups were analyzed using non-repeated measures ANOVA with Bonferroni correction. Data are representative of three independent experiments.

addition, $CD3^-$ $NK1.1^+$ cells (NK cells) in α-GCSC were also expanded 2.5-fold. To investigate whether α-GCSC containing large amounts of Vα14i NKT cells could inhibit acute GVHD, we transplanted BDF_1 mice with 7×10^7 spleen cells from B6 on day 0 for GVHD induction and α-GCSC (2×10^7 or 2×10^6 cells) on day 1. Normal mice received saline only on day 1. At day 14, mice transplanted with spleen cells from B6 mice alone (GVHD mice) exhibited donor-dominant chimerism (% donor chimerism (mean ± S.E.M.): 61.7 ± 3.0%) and expansion of donor $CD3^+$ cells (41%) including both $CD4^+$cells (25.2%) and $CD8^+$ cells (21.5%), while mice transplanted with B6 SC plus 2×10^7 α-GCSC had reduced donor chimerism (% donor chimerism (mean ± S.E.M.): 22.9 ± 5.6), lower engraftment of donor $CD4^+$ cells (12.6%) and $CD8^+$ cells (7.1%) as compared with GVHD mice (Fig. 1B and 1C). These data indicate that the transfer of α-GCSC suppressed early donor T cell engraftment. However, lower number of α-GCSC (2×10^6 cells) did not significantly inhibit donor cell engraftment (Fig. 1C).

3.2. Adoptive transfer of α-GCSC reduces symptoms of acute GVHD

Next, we examined whether the transfer of α-GCSC ameliorate serological and histological findings of acute GVHD, by analyzing the serum levels of GOT and GPT, and histology of liver tissue specimens. The serum GOT levels of GVHD mice

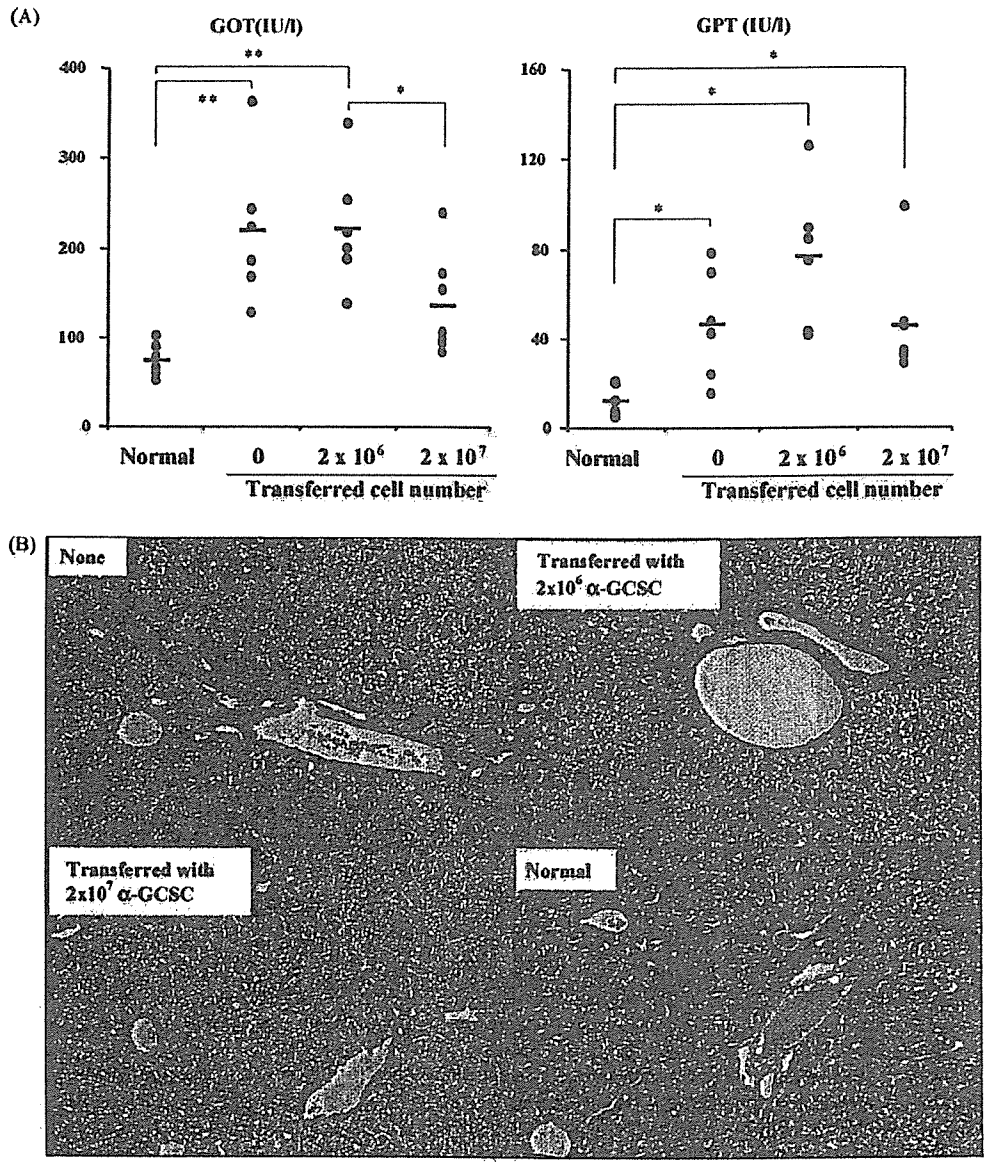

Fig. 2. Transplanted BDF_1 α-GCSC alleviated GVHD signs serologically and histologically. (A) Induction of GVHD and infusion of α-GCSC were performed as described in Fig. 1. The serum GOT levels of mice group with 2×10^7 α-GCSC were low compared with other GVHD mice groups ($^*p<0.05$ and $^{**}p<0.01$ by non-repeated measures ANOVA and Bonferroni correction), although the serum GPT levels of all mice groups were significantly high compared with normal ($n=6$). (B) Histology of liver tissue of GVHD mice with or without α-GCSC as described above and normal. Representative of three independent experiments of each group is shown.

were significantly higher as compared with untreated control mice, whereas the serum GOT levels in GVHD mice transferred with 2×10^7 α-GCSC were reduced by 50% as compared with GVHD mice (Fig. 2A). The reduction of serum GOT was not observed when transferred with 2×10^6 α-GCSC. Serum GPT levels were not significantly different among all groups (Fig. 2A). Histological analysis showed remarkable hepatic lymphocyte infiltration in the portal area in GVHD mice, while very little or no infiltration was detected in GVHD mice transferred with 2×10^7 α-GCSC. Mice treated with 2×10^6 α-GCSC showed no reduction in lymphocyte infiltration (Fig. 2B). These results indicate that α-GCSC alleviated acute GVHD and retarded donor T cell engraftment. However, spleen cells containing about 3% Vα14i NKT cells cultured with IL-2 alone could not inhibit acute GVHD and rapid donor T cell engraftment (data not shown), suggesting that the inhibitory effect of α-GCSC on GVHD is mainly attributable to the potential of Vα14i NKT cells.

3.3. Maintenance of donor cell engraftment and mixed chimerism in GVHD mice requires IL-4 but not IFN-γ following adoptive transfer of α-GCSC

Next, we examined whether the inhibition of acute GVHD was due to rapid rejection and/or graft failure by α-GCSC. Long-term donor chimerism was observed in GVHD mice with or without α-GCSC (2×10^7 cells) at 14, 42 and 100 days after the induction of GVHD (Fig. 3A). GVHD mice exhibited complete donor chimerism at day 100. Approximately 20% donor chimerism was observed in GVHD mice when treated with α-GCSC at day 14, and this gradually increased to 35% by day 100. Therefore, GVHD mice with α-GCSC sustained mixed chimerism for a significant period of time. Donor-derived lymphocytes in these mice contained T cells ($CD4^+$ and $CD8^+$) and B cells (Fig. 3B). Although very few donor-derived B cells (0.5%) were detected at 14 days after induction of GVHD with α-GCSC administration, 6% donor-derived B cells were appeared in GVHD mice with α-GCSC at 100 days. These results suggest that the transfer of α-GCSC did not impair donor cell engraftment or maintenance of long-term mixed chimerism.

It has been known that activated Vα14i NKT cells rapidly produced IL-4 and IFN-γ [23,24]. We therefore examined whether IL-4 and/or IFN-γ produced by Vα14i NKT cells is the cytokine(s) responsible for mediating inhibition of GVHD. Neutralizing mAbs against IL-4 and IFN-γ were administered intraperitoneally into GVHD mice with or without α-GCSC. As shown in Fig. 4, administration of anti-IL-4 or anti-IFN-γ mAb had no effect on donor chimerism of GVHD mice. However, the inhibitory effect on GVHD by a transfer of α-GCSC

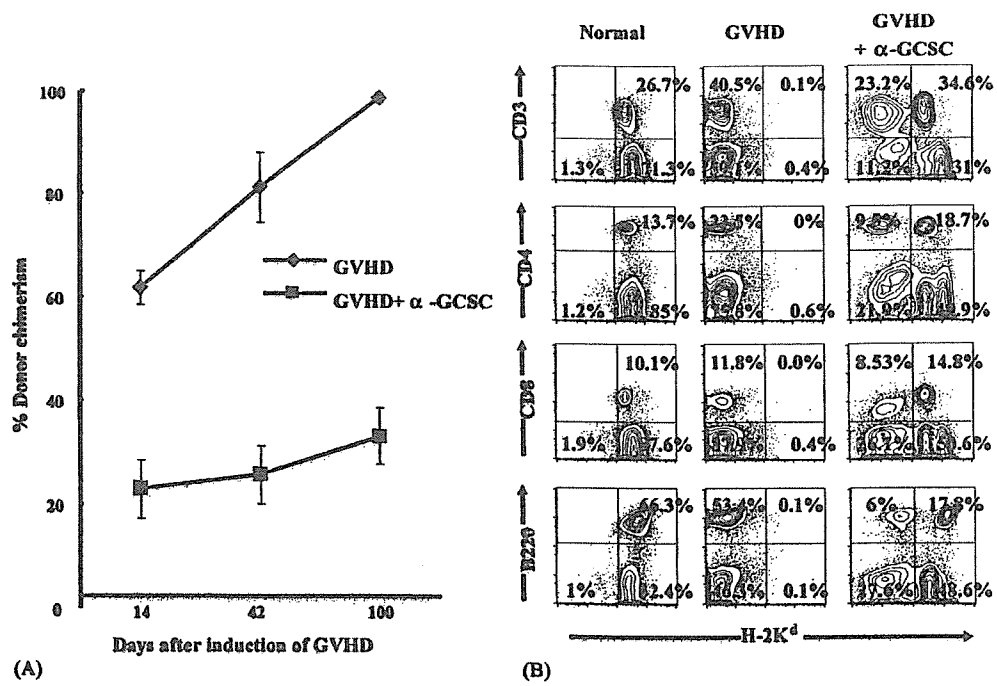

Fig. 3. Donor cells were not rejected and mixed chimerism was maintained in GVHD mice with α-GCSC for a long term. (A) Induction of GVHD and a transfer of α-GCSC were performed as described in Fig. 1. SC of GVHD mice transplanted with or without α-GCSC were stained with anti-H-$2K^b$ mAb and then donor chimerism was determined on days 14, 42 and 100 after GVHD induction. Percentages of donor chimerism in SC of GVHD mice transplanted with α-GCSC gradually increased as days passed. GVHD indicates GVHD mice without transfer of α-GCSC ($n=6$ on day 14, $n=6$ on day 42, $n=4$ on day 100); GVHD + cultured SC, GVHD mice with transfer of α-GCSC ($n=7$ on day 14, $n=5$ on day 42, $n=4$ on day 100). Values are mean ± S.E.M. on days 14, 42 and 100. $^{**}p<0.01$ versus group of GVHD. (B) SC of untreated (normal: the left column), transplanted with B6 SC alone (GVHD: the center) and transplanted with both B6 SC and 2×10^7 α-GCSC (GVHD + cultured SC: the right) mice were stained with anti-H-$2K^d$-FITC and each of anti-CD3, CD4, CD8, B220, DX-5-PE mAb on day 100. The numbers in each of the quadrants represent the percentage of total analyzed cells. The fluorescence profiles are representative of at least three independent experiments.

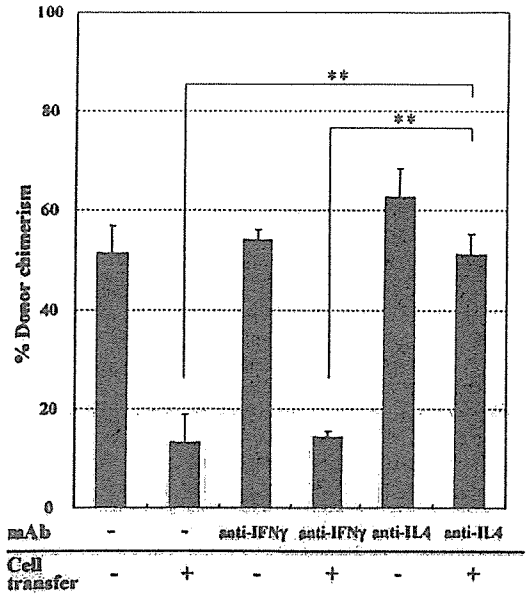

Fig. 4. GVHD was inhibited by the function of BDF_1 α-GCSC depending on IL-4, but not IFN-γ. Induction of GVHD and a transfer of α-GCSC were performed as described in Fig. 1. GVHD mice with or without α-GCSC were injected with or without anti-IL-4 (3 mg/mouse) or IFN-γ (1 mg/mouse) neutralizing mAbs on day 1. Donor chimerism was determined by anti-H-$2K^b$ mAb on day 14. Values are mean ± SEM on day 14. The number of each group is from the left $n = 5, 6, 6, 4, 4$ and 5, respectively.

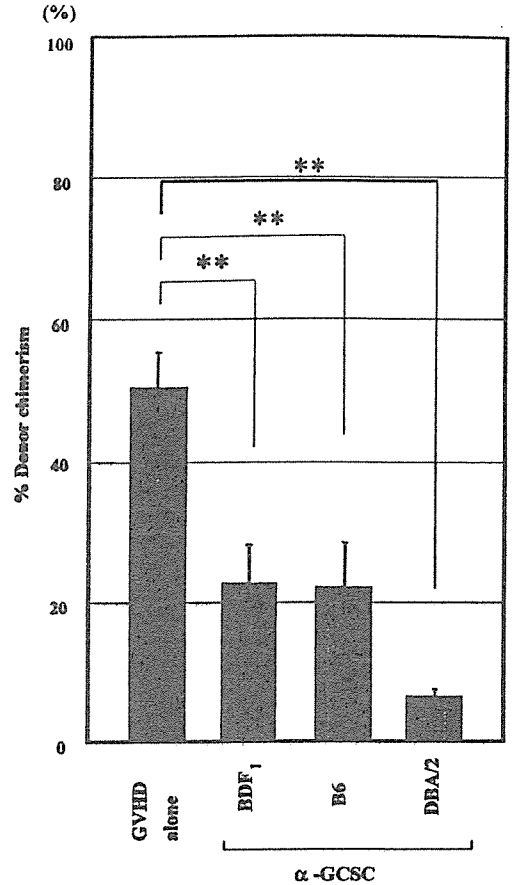

Fig. 5. α-GCSC from B6 or DBA/2 mice could also inhibit GVHD. Induction of GVHD and infusion of α-GCSC were performed as described in Fig. 1. The percentages of donor cell chimerism at day 14 in GVHD mice with any α-GCSC was significantly lower compared with GVHD mice with none (GVHD). The number of each group is GVHD (GVHD mice with none), $n = 15$; BDF_1, $n = 7$; B6, $n = 6$; DBA/2, $n = 6$. $^{**}p < 0.01$ versus group of GVHD by non-repeated measures ANOVA and Bonferroni correction.

was blocked by anti-IL-4, but not by anti-IFN-γ mAb (Fig. 4). Therefore, the retardation of donor cell engraftment and alleviation of acute GVHD by α-GCSC appears to be mediated by an IL-4-dependent mechanism.

3.4. Purified in vitro-expanded Vα14i NKT cells ameliorated acute GVHD

We next determined whether α-GCSC derived from the parental strain (B6 or DBA/2) could also inhibit rapid donor cell engraftment. Firstly, α-GCSC containing 30 or 15% of Vα14i NKT cells in B6 mice or DBA/2 mice, respectively, were transferred (2×10^7) into GVHD mice. Expectedly, transfer of α-GCSC, originating from both B6 and DBA/2 mice reduced the percentage of donor chimerism in GVHD mice (Fig. 5). The results suggest that the inhibitory effect of α-GCSC on GVHD was not related to their strain of origin.

To examine which cell compartment in the α-GCSC inhibits acute GVHD, Vα14i NKT cells were purified from α-GCSC by using CD1d/α-GalCer tetramer and MACS system. The purity of Vα14i NKT cells was more than 96% (Fig. 6A). Donor chimerism of GVHD mice injected with 4×10^6 purified Vα14i NKT cells (nearly equivalent to 2×10^7 α-GCSC) was lower than that of mice with GVHD alone, although it was higher than that of GVHD mice transplanted with 2×10^7 of α-GCSC (Fig. 6B). This data indicates that transfer of purified Vα14i NKT cells alone can ameliorate GVHD.

4. Discussion

Vα14i NKT cells play an important role in immune regulation including autoimmunity, tumor immunity and infection. Furthermore, it has been demonstrated that $NK1.1^+$ NKT cells from donor bone marrow [5] or residual host [30] can inhibit acute GVHD. Recently, several groups reported that *in vivo* administration of the Vα14i NKT cell specific ligand, α-GalCer, modulated acute GVHD and prolonged survival [13,14,31]. These studies suggest the therapeutic potential of α-GalCer or Vα14i NKT cells for the prevention of acute GVHD after allogeneic HSCT.

Although we also obtained similar results regarding the inhibition of GVHD by α-GalCer-activated Vα14i NKT cells, we used *in vitro*-expanded Vα14i NKT cells and non-myeloablative F_1 mice as recipients. It is likely that this difference led to the distinct results in regard to the difference in donor chimerism. We found that GVHD mice with a transfer of Vα14i NKT cells could maintain mixed chimerism (donor chimerism frequency of 20–30%) for a long period. By contrast, Morecki et al. trans-

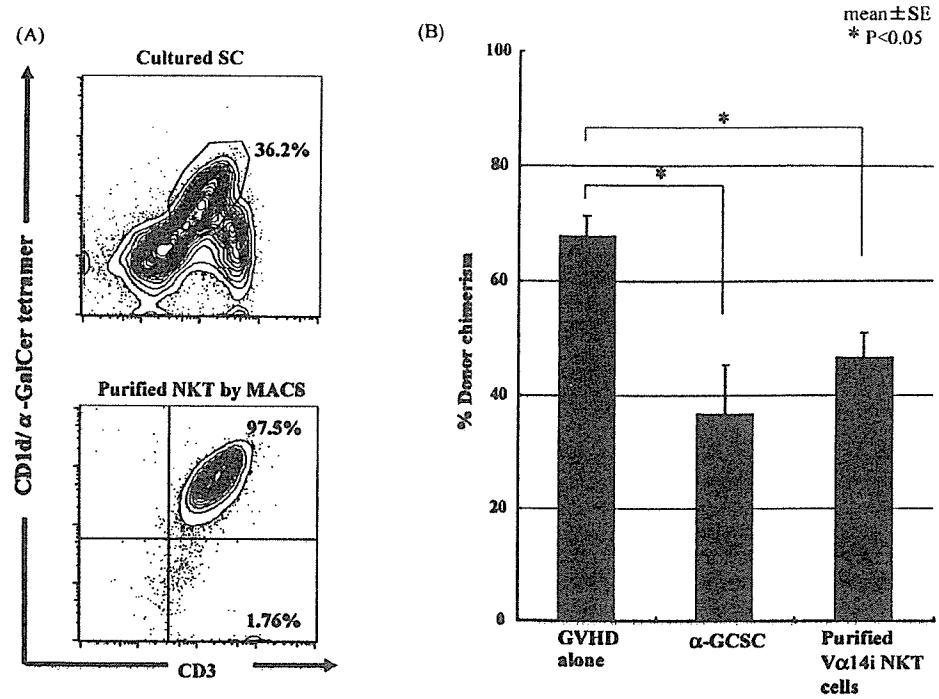

Fig. 6. Purified Vα14i NKT cells from BDF_1 α-GCSC also alleviated GVHD. (A, B) Induction of GVHD and cell culture were performed as described in Fig. 1. The purification of NKT cells from BDF_1 α-GCSC was done as described in materials and methods. (A) Before and after the purification of NKT cells, BDF_1 α-GCSC were stained with anti-CD3-FITC and CD1d/α-GalCer tetramer-APC or CD1d/α-GalCer tetramer-PE mAb. The numbers in each of the quadrants represent the percentage of total analyzed cells. The fluorescence profiles are representative of at least three independent experiments. (B) Mice were additionally infused with or without 2×10^7 BDF_1 α-GCSC or 4×10^6 purified NKT cells from α-GCSC by MACS system. The percentage of donor cell chimerism in SC in each mouse was determined on day 14. The number of each group is GVHD (GVHD mice with none), $n=6$; α-GCSC 2×10^7, $n=5$; isolated Vα14i NKT cells 4×10^6, $n=6$. $^{**}p<0.01$ versus group of GVHD by non-repeated measures ANOVA and Bonferroni correction.

planted spleen cells of parental B6 mice into low dose total body irradiated (BALB/c × B6) F_1 mice similar to our GVHD model and showed that the donor chimerism of α-GalCer- administered mice was very low (2% of donor chimerism). This difference in donor chimerism between a transfer of Vα14i NKT cells and an injection with α-GalCer seems to be attributable to IL-4, although previous studies [14,31] and our current results demonstrated that IL-4 from Vα14i NKT cells mainly contributed to the inhibition of acute GVHD. It has been reported that the amount and time course of serum IL-4 levels were distinct between direct administration of α-GalCer and the transfer of α-GalCer pulsed dendritic cells [32]. Direct administration of α-GalCer induced more rapid and higher levels of serum IL-4 levels as compared with α-GalCer-pulsed dendritic cells. We propose that the distinct donor chimerism in GVHD mice between a transfer of Vα14i NKT cells and an injection with α-GalCer may be attributable to the different amount and time course of serum IL-4 levels. Furthermore, we measured Th polarization (IL-4 and IFN-γ production) in total (donor plus recipient) cells 7 days after transplantation by ELISA assay and found a Th2 dominant response (data not shown). However, we do not know if a Th2 dominant response differed between donor and recipient derived cells.

Previous reports [29,33,34] indicated that rapid engraftment of donor cells was always accompanied by severe GVHD, and that, conversely, slow engraftment led to a reduction of GVHD. Pan et al. [35] also showed that a stable and lower level of donor chimerism should be enough to induce donor–recipient reciprocal tolerance. Thus, their and our data show that IL-4-dependent retention of mixed chimerism or a gradual transition from a mixed to a complete chimera by transfer of α-GCSC leads to alleviation of GVHD. It should be noted, however, that systemic administration of IL-4 is ineffective or toxic [36]. Moreover, a stable mixed chimerism of GVHD mice transplanted with Vα14i NKT cells was sustained for an expanded period. These results suggest that the stable chimerism induced by Vα14i NKT cells is not due to graft rejection.

α-GCSC including $CD1d^+$ cells loaded with α-GalCer activated recipient Vα14i NKT cells (data not shown). Therefore, both recipient and transferred Vα14i NKT cells might contribute to alleviation of GVHD as previously reported [31]. However, we showed that inhibition of GVHD by Vα14i NKT cells was due to IL-4 produced exclusively by Vα14i NKT cells among α-GCSC [24], and that a transfer of purified Vα14i NKT cells alone prevented acute GVHD. These data suggest that transferred Vα14i NKT cells were sufficient to modulate acute GVHD.

Recently, Haraguchi et al. [31] reported the effect of *in vivo* administration of α-GalCer and the adoptive transfer of NKT cells on the prevention of GVHD. This seems to be logical considering the relationship between host-residual and transferred NKT cells as they mentioned that host-residual, but not

transferred, NKT cells are essential for amelioration of GVHD. Although the authors indicated that maximal GVHD reduction and survival were mainly accompanied by graft rejection, our data demonstrated that effective GVHD reduction was accompanied by maintenance of mixed chimerism. This discrepancy may be explained by the different GVHD settings, non-myeloablative and myeloablative recipients, and by the balance between the dose of alloreactive donor cells and the activity of host-residual NKT cells.

Although several studies have reported that the number of circulating NKT cells was reduced in cancer patients [17,37,38], direct injection of α-GalCer is not expected to induce anti-tumor effects. On the other hand, adoptive *in vitro*-expanded NKT cell immunotherapy may be useful for cancer therapy. In support of this, we found that adoptive transfer of *in vitro*-expanded Vα14i NKT cells could prevent lung tumor metastasis in a mouse model (unpublished data Ikarashi et al.). We believe that adoptive transfer of NKT cell therapy combined with allogenic HSCT may be beneficial for cancer patients, because of NKT cell function for prevention of GVHD and anti-tumor effects.

Acknowledgments

We thank Pharmaceutical Research Laboratory, Kirin Brewery Co. (Gumma, Japan) for providing α-GalCer and thank Dr. Kazuyoshi Takeda (Juntendo University, Tokyo, Japan) for providing hybridoma cell lines. This work was supported in part by a grant-in-aid for the Third-Term Comprehensive 10-Year Strategy for Cancer Control from the Ministry of Health, Labour and Welfare, Japan and Research Resident Fellowship from the Foundation for Promotion of Cancer Research, Japan (M. Kuwatani).

References

[1] Kawano T, Cui J, Koezuka Y, Toura I, Kaneko Y, Motoki K, et al. CD1d-restricted and TCR-mediated activation of Vα14 NKT cells by glycosylceramides. Science 1997;278:1626–9.

[2] Hammond KJ, Poulton LD, Palmisano LJ, Silveira PA, Godfrey DI, Baxter AG. α/β-T cell receptor (TCR)$^+$CD4$^-$CD8$^-$ (NKT) thymocytes prevent insulin-dependent diabetes mellitus in non-obese diabetic (NOD)/Lt mice by the influence of interleukin (IL)-4 and/or IL-10. J Exp Med 1998;187:1047–56.

[3] Moodycliffe AM, Nghiem D, Clydesdale G, Ullrich SE. Immune suppression and skin cancer development: regulation by NKT cells. Nat Immunol 2000;1:521–5.

[4] Kikuchi A, Nieda M, Schmidt C, Koezuka Y, Ishihara S, Ishikawa Y, et al. *In vitro* anti-tumor activity of α-galactosylceramide-stimulated human invariant Vα24$^+$ NKT cells against melanoma. Br J Cancer 2001;85:741–6.

[5] Zeng D, Lewis D, Dejbakhsh-Jones S, Lan F, Garcia-Ojeda M, Sibley R, et al. Bone marrow NK1.1$^-$ and NK1.1$^+$ T cells reciprocally regulate acute graft-versus-host disease. J Exp Med 1999;189:1073–81.

[6] Burnett AK, Hann IM, Robertson AG, Alcorn M, Gibson B, McVicar I, et al. Prevention of graft-versus-host disease by *in vitro* T cell depletion: reduction in graft failure with augmented total body irradiation. Leukemia 1988;2:300–3.

[7] Deeg HJ. Prophylaxis and treatment of acute graft-versus-host disease: current state, implications of new immunopharmacologic compounds and future strategies to prevent and treat acute GVHD in high-risk patients. Bone Marrow Transplant 1994;14(Suppl 4):S56–60.

[8] Via CS, Sharrow SO, Shearer GM. Role of cytotoxic T lymphocytes in the prevention of lupus-like disease occurring in a murine model of graft-versus-host disease. J Immunol 1987;139:1840–9.

[9] Rus V, Svetic A, Nguyen P, Gause WC, Via CS. Kinetics of Th1 and Th2 cytokine production during the early course of acute and chronic murine graft-versus-host disease. Regulatory role of donor CD8$^+$ T cells. J Immunol 1995;155:2396–406.

[10] Allen RD, Staley TA, Sidman CL. Differential cytokine expression in acute and chronic murine graft-versus-host-disease. Eur J Immunol 1993;23:333–7.

[11] Edinger M, Hoffmann P, Ermann J, Drago K, Fathman CG, Strober S, et al. CD4$^+$CD25$^+$ regulatory T cells preserve graft-versus-tumor activity while inhibiting graft-versus-host disease after bone marrow transplantation. Nat Med 2003;9:1144–50.

[12] Baker J, Verneris MR, Ito M, Shizuru JA, Negrin RS. Expansion of cytolytic CD8$^+$ natural killer T cells with limited capacity for graft-versus-host disease induction due to interferon γ production. Blood 2001;97:2923–31.

[13] Morecki S, Panigrahi S, Pizov G, Yacovlev E, Gelfand Y, Eizik O, et al. Effect of KRN7000 on induced graft-vs-host disease. Exp Hematol 2004;32:630–7.

[14] Hashimoto D, Asakura S, Miyake S, Yamamura T, Van Kaer L, Liu C, et al. Stimulation of host NKT cells by synthetic glycolipid regulates acute graft-versus-host disease by inducing Th2 polarization of donor T cells. J Immunol 2005;174:551–6.

[15] Godfrey DI, Hammond KJ, Poulton LD, Smyth MJ, Baxter AG. NKT cells: facts, functions and fallacies. Immunol Today 2000;21:573–83.

[16] Haraguchi K, Takahashi T, Hiruma K, et al. Recovery of Vα24$^+$ NKT cells after hematopoietic stem cell transplantation. Bone Marrow Transplant 2004;34:595–602.

[17] Giaccone G, Punt CJ, Ando Y, Ruijter R, Nishi N, Peters M, et al. A phase I study of the natural killer T-cell ligand α-galactosylceramide (KRN7000) in patients with solid tumors. Clin Cancer Res 2002;8:3702–9.

[18] Nieda M, Okai M, Tazbirkova A, Lin H, Yamaura A, Ide K, et al. Therapeutic activation of Vα24$^+$Vβ11$^+$ NKT cells in human subjects results in highly coordinated secondary activation of acquired and innate immunity. Blood 2004;103:383–9.

[19] Lin H, Nieda M, Nicol AJ. Differential proliferative response of NKT cell subpopulations to *in vitro* stimulation in presence of different cytokines. Eur J Immunol 2004;34:2664–71.

[20] Brossay L, Chioda M, Burdin N, Koezuka Y, Casorati G, Dellabona P, et al. CD1d-mediated recognition of an α-galactosylceramide by natural killer T cells is highly conserved through mammalian evolution. J Exp Med 1998;188:1521–8.

[21] Nishi N, van der Vliet HJ, Koezuka Y, von Blomberg BM, Scheper RJ, Pinedo HM, et al. Synergistic effect of KRN7000 with interleukin-15, -7, and -2 on the expansion of human Vα 24$^+$Vβ 11$^+$ T cells *in vitro*. Hum Immunol 2000;61:357–65.

[22] van der Vliet HJ, Nishi N, Koezuka Y, von Blomberg BM, van den Eertwegh AJ, Porcelli SA, et al. Potent expansion of human natural killer T cells using α-galactosylceramide (KRN7000)-loaded monocyte-derived dendritic cells, cultured in the presence of IL-7 and IL-15. J Immunol Meth 2001;247:61–72.

[23] Kronenberg M, Gapin L. The unconventional lifestyle of NKT cells. Nat Rev Immunol 2002;2:557–68.

[24] Ikarashi Y, Iizuka A, Heike Y, Yoshida M, Takaue Y, Wakasugi H. Cytokine production and migration of in-vitro expanded NK1.1$^-$ invariant Vα14 natural killer T (Vα14i NKT) cells using α-galactosylceramide and IL-2. Immunol Lett 2005;101:160–7.

[25] Matsuda JL, Naidenko OV, Gapin L, Nakayama T, Taniguchi M, Wang CR, et al. Tracking the response of natural killer T cells to a glycolipid antigen using CD1d tetramers. J Exp Med 2000;192:741–54.

[26] Yoshino S, Murata Y, Ohsawa M. Successful induction of adjuvant arthritis in mice by treatment with a monoclonal antibody against IL-4. J Immunol 1998;161:6904–8.

[27] Puliaev R, Nguyen P, Finkelman FD, Via CS. Differential requirement for IFN-γ in CTL maturation in acute murine graft-versus-host disease. J Immunol 2004;173:910–9.
[28] Carnaud C, Lee D, Donnars O, Park SH, Beavis A, Koezuka Y, et al. Cutting edge: cross-talk between cells of the innate immune system: NKT cells rapidly activate NK cells. J Immunol 1999;163:4647–50.
[29] Xun CQ, Tsuchida M, Thompson JS. Delaying transplantation after total body irradiation is a simple and effective way to reduce acute graft-versus-host disease mortality after major H2 incompatible transplantation. Transplantation 1997;64:297–302.
[30] Lan F, Zeng D, Higuchi M, Huie P, Higgins JP, Strober S. Predominance of NK1.1$^+$TCRαβ$^+$ or DX5$^+$TCRαβ$^+$ T cells in mice conditioned with fractionated lymphoid irradiation protects against graft-versus-host disease: "natural suppressor" cells. J Immunol 2001;167:2087–96.
[31] Haraguchi K, Takahashi T, Matsumoto A, Asai T, Kanda Y, Kurokawa M, et al. Host-residual invariant NK T cells attenuate graft-versus-host immunity. J Immunol 2005;175:1320–8.
[32] Fujii S, Shimizu K, Kronenberg M, Steinman RM. Prolonged IFN-γ-producing NKT response induced with α-galactosylceramide-loaded DCs. Nat Immunol 2002;3:867–74.
[33] Ritchie DS, Morton J, Szer J, Robert AW, Durrant S, Shuttleworth P, et al. Graft-versus-host disease, donor chimerism, and organ toxicity in stem cell transplantation after conditioning with fludarabine and melphalan. Biol Blood Marrow Transplant 2003;9:435–42.
[34] Childs R, Clave E, Contentin N, Jayasekera D, Hensel N, Leitman S, et al. Engraftment kinetics after non-myeloablative allogeneic peripheral blood stem cell transplantation: full donor T-cell chimerism precedes alloimmune responses. Blood 1999;94:3234–41.
[35] Pan Y, Luo B, Sozen H, Kalscheuer H, Blazar BR, Sutherland DE, et al. Blockade of the CD40/CD154 pathway enhances T-cell-depleted allogeneic bone marrow engraftment under non-myeloablative and irradiation-free conditioning therapy. Transplantation 2003;76:216–24.
[36] Atkinson K, Matias C, Guiffre A, Seymour R, Cooley M, Biggs J, et al. In vivo administration of granulocyte colony-stimulating factor (G-CSF), granulocyte-macrophage CSF, interleukin-1 (IL-1), and IL-4, alone and in combination, after allogeneic murine hematopoietic stem cell transplantation. Blood 1991;77:1376–82.
[37] Motohashi S, Kobayashi S, Ito T, Magara KK, Mikuni O, Kamada N, et al. Preserved IFN-α production of circulating Vα24 NKT cells in primary lung cancer patients. Int J Cancer 2002;102:159–65.
[38] Molling JW, Kolgen W, van der Vliet HJ, Boomsma MF, Kruizenga H, Smorenburg CH, et al. Peripheral blood IFN-γ-secreting Vα24$^+$Vβ11$^+$ NKT cell numbers are decreased in cancer patients independent of tumor type or tumor load. Int J Cancer 2005;116:87–93.

Efficient Ex vivo Expansion of Vα24$^+$ NKT Cells Derived From G-CSF-mobilized Blood Cells

Osamu Imataki,†§ Yuji Heike,*† Toshihiko Ishida,§ Yoichi Takaue,* Yoshinori Ikarashi,† Mitsuji Yoshida,† Hiro Wakasugi,† and Tadao Kakizoe#*

Summary: Natural killer T (NKT) cells are involved in the function of innate immune systems and also play an important role in regulating acquired immune responses. In previous reports, we showed that Vα24$^+$ NKT cells proliferated more efficiently from granulocyte-colony stimulating factor (G-CSF)-mobilized peripheral blood mononuclear cells (PBMC) than from non-mobilized PBMC. However, the mechanism of this enhanced NKT cell expansion is not yet clear. The goal of this research was to develop culture conditions for the more efficient ex vivo expansion of NKT cells. G-CSF-mobilized PBMC was cultured in AIM-V medium supplemented with 10% autoplasma, 100 ng/mL α-galactosylceramide (α-GalCer) and 100 IU/mL recombinant human (rh) interleukin (IL)-2. The efficiency of the expansion of Vα24$^+$ NKT cells was evaluated on day 12. The expansion-fold of Vα24$^+$ NKT cells was augmented depending on the proportion of CD14$^+$ cells at the beginning of culture. The depletion of Vα24$^+$ NKT cells abrogated the expansion of Vα24$^+$ NKT cells. Depletion of CD56$^+$ NK cells from mobilized PBMC enhanced, and add-back of purified CD56$^+$ NK cells suppressed the expansion of Vα24$^+$ NKT cells. Experiments with different timings for the addition of cells, IL-2 and α-GalCer suggested that follow-up supplementation with IL-2 or CD14$^+$ cells should be avoided for the efficient expansion of Vα24$^+$ NKT cells. These results should be useful for the development of an efficient and practical expansion protocol for adoptive immunotherapy with Vα24$^+$ NKT cells.

Key Words: Vα24$^+$ NKT cells, α-galactosylceramide, CD14$^+$ cells, CD56$^+$ NK cells

(*J Immunother* 2006;29:320–327)

Received for publication September 28, 2005; accepted November 8, 2005.

From the †Pharmacology Division, National Cancer Center Research Institute, Tokyo, Japan; *Blood and Stem Cell Transplantation Unit, National Cancer Center Hospital, Tokyo, Japan; §First Department of Internal Medicine, Kagawa Medical University Hospital, Kagawa, Japan; and #President, National Cancer Center, Tokyo, Japan.

This research was supported by a Grant-in-Aid for Scientific Research from the Ministry of Health, Labor and Welfare and a Grant from the Advanced Clinical Research Organization.

Reprints: Yuji Heike, MD, PhD, Pharmacology Division, National Cancer Center Research Institute, 5-1-1, Tsukiji, Chuo-Ku, Tokyo, 104-0045, Japan (e-mail: yheike@ncc.go.jp).

INTRODUCTION

NKT cells are lymphocyte lineage and show characteristics of both T cells and NK cells.[1] NKT cells coexpress T cell receptors (TCRs) and NK cell markers, and display an extremely restricted TCR repertoire, consisting of Vα24 chain preferentially paired with V_β11 chain. Upon activation by a specific ligand, NKT cells produce high levels of interferon-gγ (IFN-γ) and interleukin-4 (IL-4), and yield a strong immune response against several types of tumor cells.[2] Therefore, these invariant NKT cells are considered key effector cells, and play critical roles in immunity against microbial infection, tumor and autoantigens.

The marine sponge-derived glycosphingolipid α-galactosylceramide (α-GalCer) specifically activates human and mouse invariant NKT cells.[3,4] In vivo activation of NKT cells by α-GalCer induced strong cytotoxicity and the production of several cytokines in mice,[5] and it is well known that NKT cells differentiate efficiently with the in vitro administration of α-GalCer to acquire cytotoxic activities.[6] Therefore, this glycolipid agent may be able to effectively expand and activate NKT cells, and thus may be a useful tool for clinical immunotherapy.

For the clinical application of NKT cells in cancer immunotherapy, efficient expansion of the cells is very important. We previously reported that granulocyte colony-stimulating factor (G-CSF)-mobilized PBMC showed a higher efficacy of expansion of NKT cells,[7] and a fetal bovine serum (FBS)-free culture system has been developed.[8] In this study, we further attempted to improve the culture system by evaluating the effects of other cell components and interleukin (IL)-2.

MATERIALS AND METHODS

Cells and Plasma Preparation

Peripheral blood (PB) or apheresis products were obtained from normal healthy donors for allogeneic peripheral blood stem cell transplantation (PBSCT) after written informed consent was obtained. Healthy donors were administered G-CSF (filgrastim) 10 μg/kg subcutaneously for 4 continuous days, and leukapheresis was performed on the 4th day. PB was collected in a heparin-containing collection tube before and after G-CSF mobilization. The plasma was separated from cell components by centrifugation at 3,000 rpm for 15